SAND2015-8494C

Exceptional service in the national interest

Sandia National Laboratories

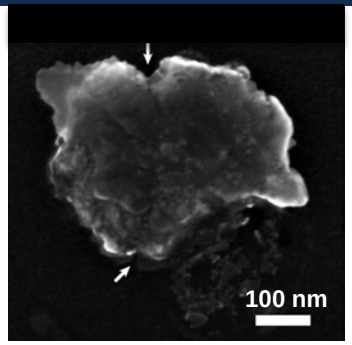

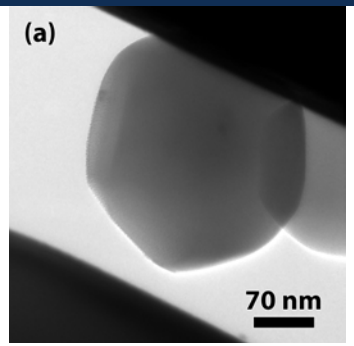

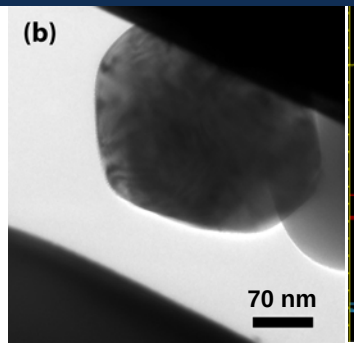

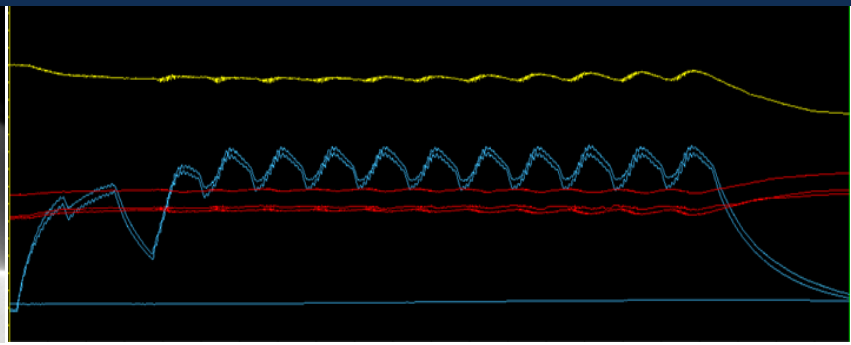

Thermal Spray Research at Sandia

Deidre Hirschfeld, Pylin Sarobol, Andrew Miller, Aaron Hall, Thomas Holmes, and Carlos Silva

ITSA, Oct 2, 2015

U.S. DEPARTMENT OF ENERGY | NNSA National Nuclear Security Administration

Sandia National Laboratories is a multi-program laboratory managed and operated by Sandia Corporation, a wholly owned subsidiary of Lockheed Martin Corporation, for the U.S. Department of Energy's National Nuclear Security Administration under contract DE-AC04-94AL85000. SAND2015-3704C

Thermal Spray at Sandia

Sandia National Laboratories

- Development of Thermal Spray Technologies
  - Plasma Spray, CAPS (VPS, VLPPS)
  - TWA
  - Cold Spray
  - HVOF
  - Powder Flame Spray
  - Aerosol Deposition
- Highlight Recent Work
  - Diagnostics: Use of Control Vision, DPV, and ICP
  - Aerosol Deposition: Deformation Mechanisms

Plasma Spray Processes

Sandia National Laboratories

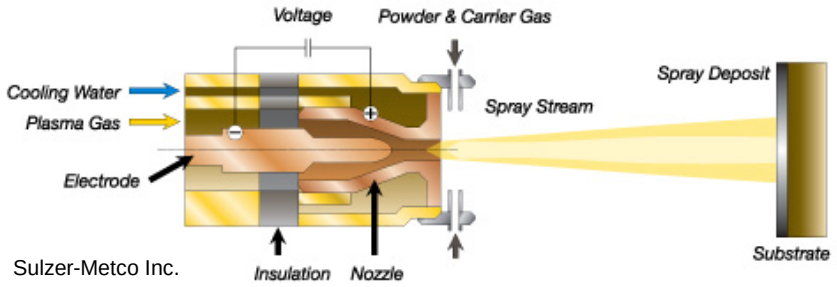

Sulzer-Metco Inc.

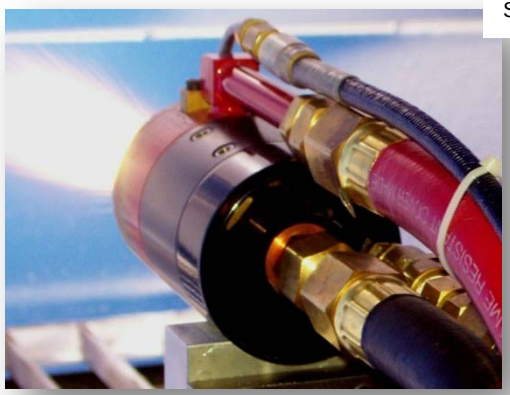

SG-100 Praxair-Tafa Inc.

Air Plasma Spray
- DC Plasma heat source
- SG-100, Triplex®Pro-200
- I, V, & Gas Composition affect T_p & V_p

"Vacuum" Plasma Spray
- Plasma spray at ~ ½ atmosphere (380 torr)
- Oxide-free coatings

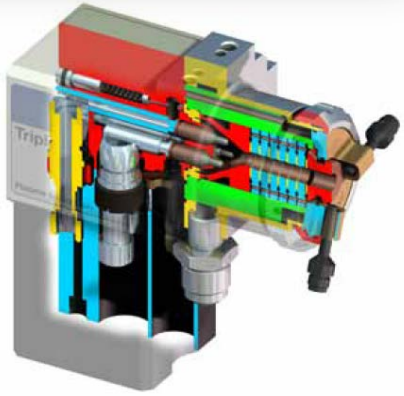

Triple cathode design

Triplex®Pro-200 Sulzer-Metco Inc.

Very Low Pressure Plasma Spray
- Plasma spray at 1.0 Torr (0.001 atm)
- Emerging Technology
- SNL has one of two systems in U.S.
- *Droplet Deposition*
- *Vapor Deposition!*
- *Thin coatings (< 50 microns)*

O3CA Suzler-Metco Inc.

Measuring the parameters between torch and substrate

DIAGNOSTICS: TUNING THE PROCESS

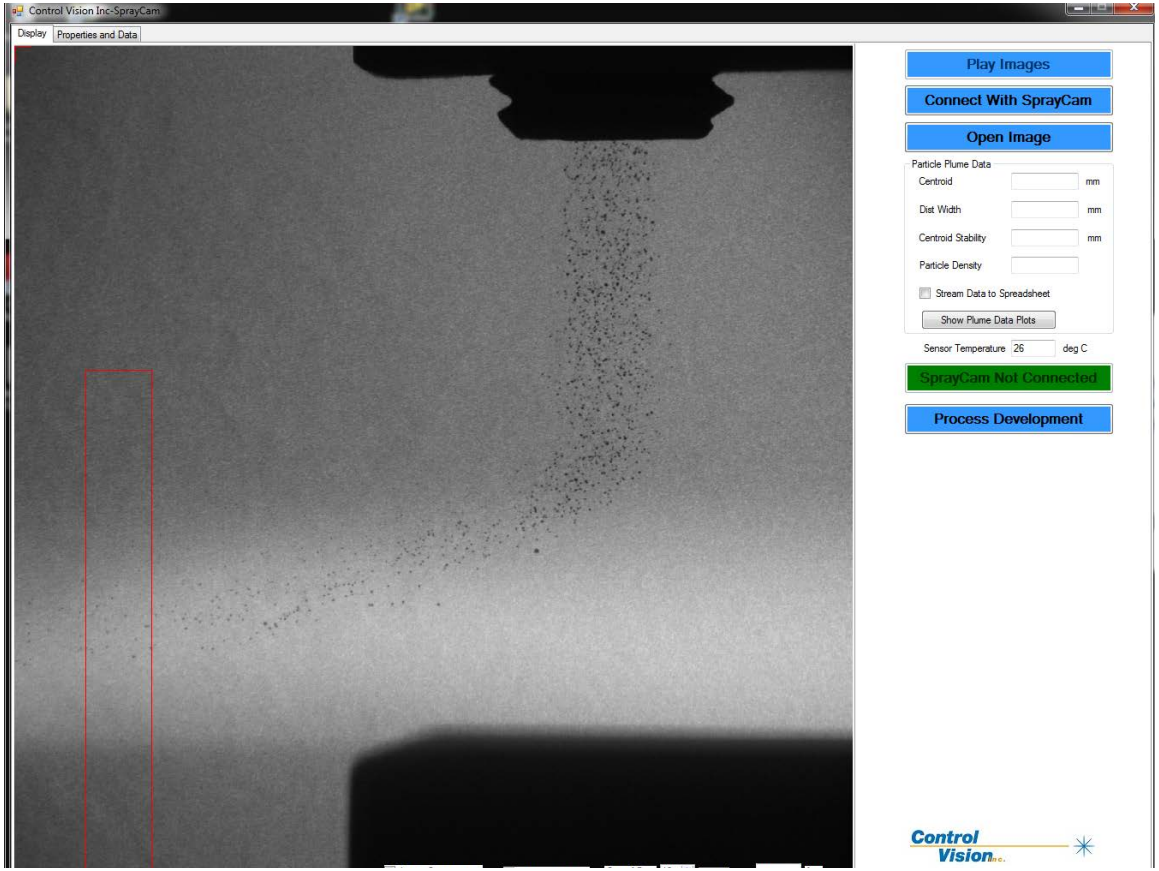

Control Vision

- Optimize particle insertion to the plume
- Quantify flux at a point in the plume

Particle Temperature (Tp) and Particle Velocity (Vp) directly affect coating microstructure and properties.

Sandia National Laboratories

Tp: Particle Thermal energy
Vp: Particle Kinetic energy

- *Are controllable*
- *Are measureable*
- *Make sense*

Increasing Tp or Vp

- *Increases deposition efficiency*
- *Reduces coating porosity*
- *May increase residual stress*
- *May increase substrate damage*

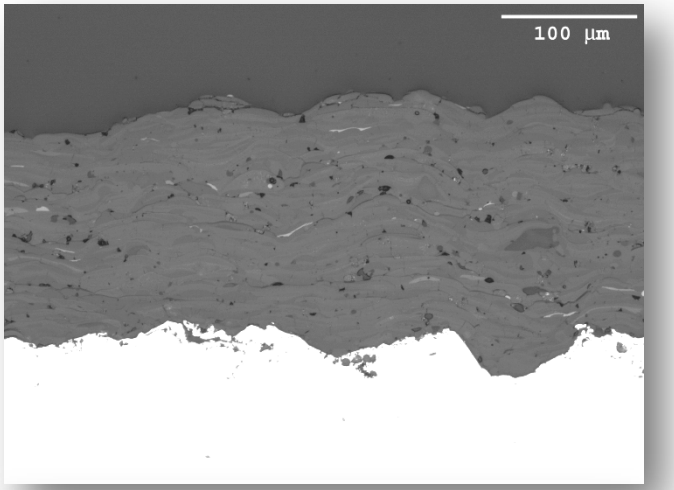

VS.

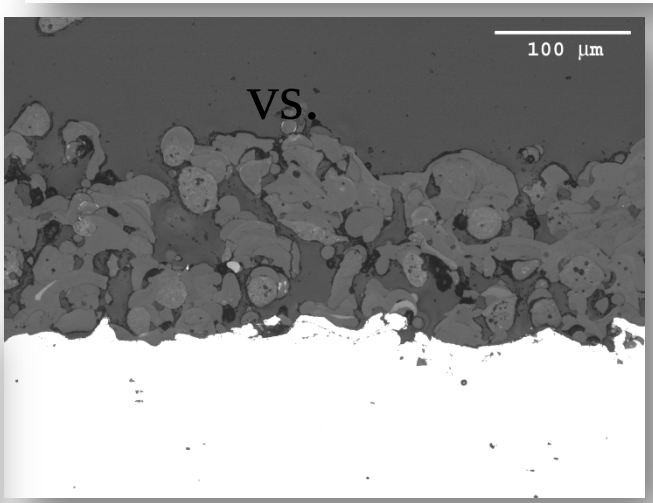

Sensor-Based Particle Characterization

- *Simultaneous time of flight and two color pyrometry measurement*

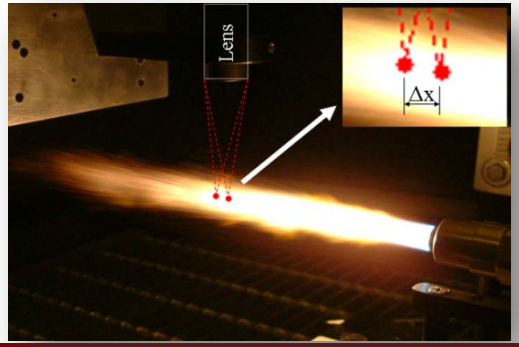

$Vp = \Delta x / \Delta t$

$Tp = \lambda 1 / \lambda 2$

DPV Histogram

Precise measurement of velocity and temperature of up to 4000 individual particles per second

Auto-center function ensures measurement is centered on point of highest particle flux

Measurement taken at specified standoff distance provides details about particle state at impact plane

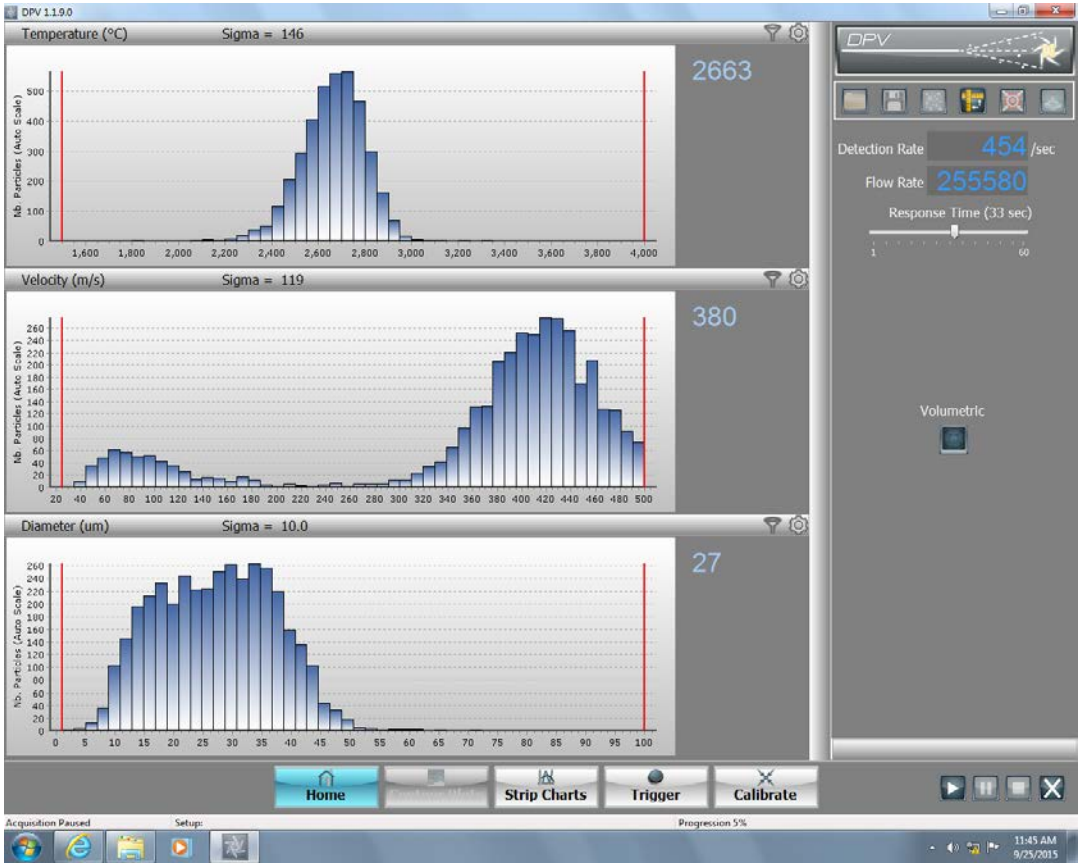

DPV Contour

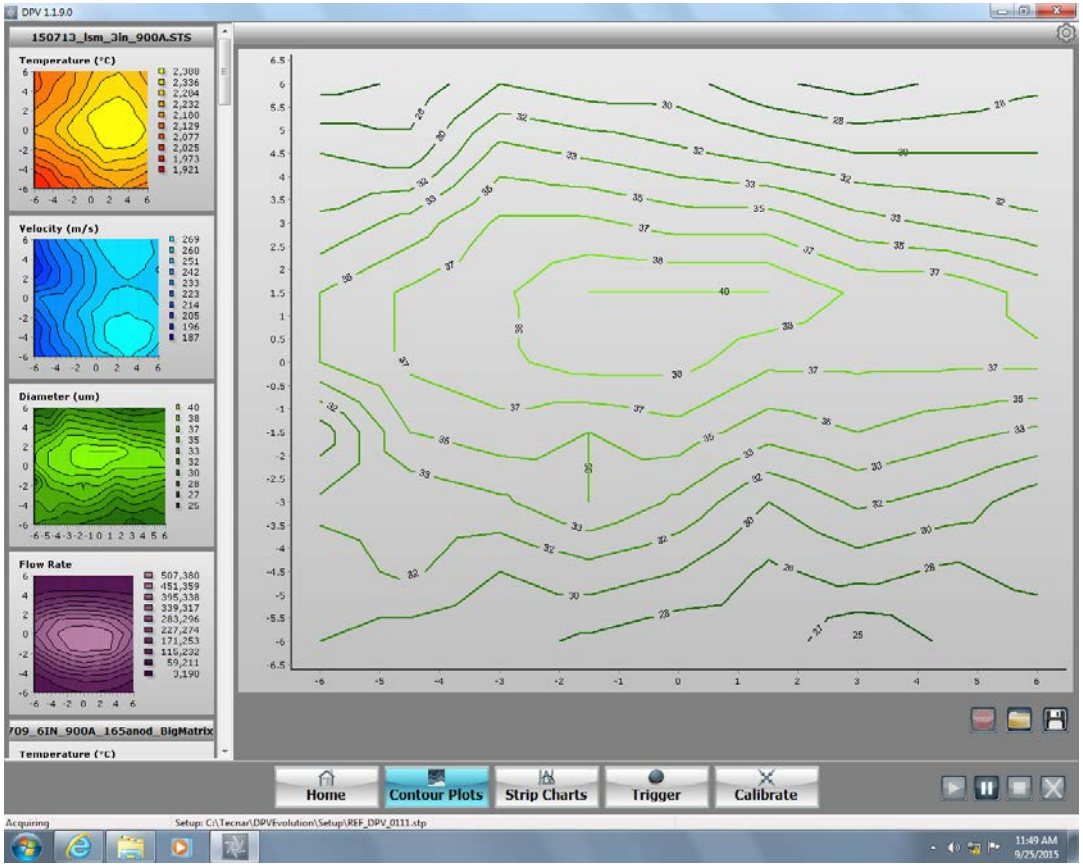

Temp, Velocity, Particle Diameter, Particle Flow Rate at specified standoff distance

Less precise than histogram

How can we know that one coating is the same as another?

MEASURING COATINGS IN-SITU

Motivation

New instrument measures curvature and temperature real time, in-situ to determine residual stress and elastic modulus of sprayed coating

In-situ coating properties (ICP) sensor can be used to determine repeatability of coating based on these parameters with much faster turn around.

Limitations of the instrument require knowledgeable user and some institutional experience to effectively quantify and produce repeatable coatings

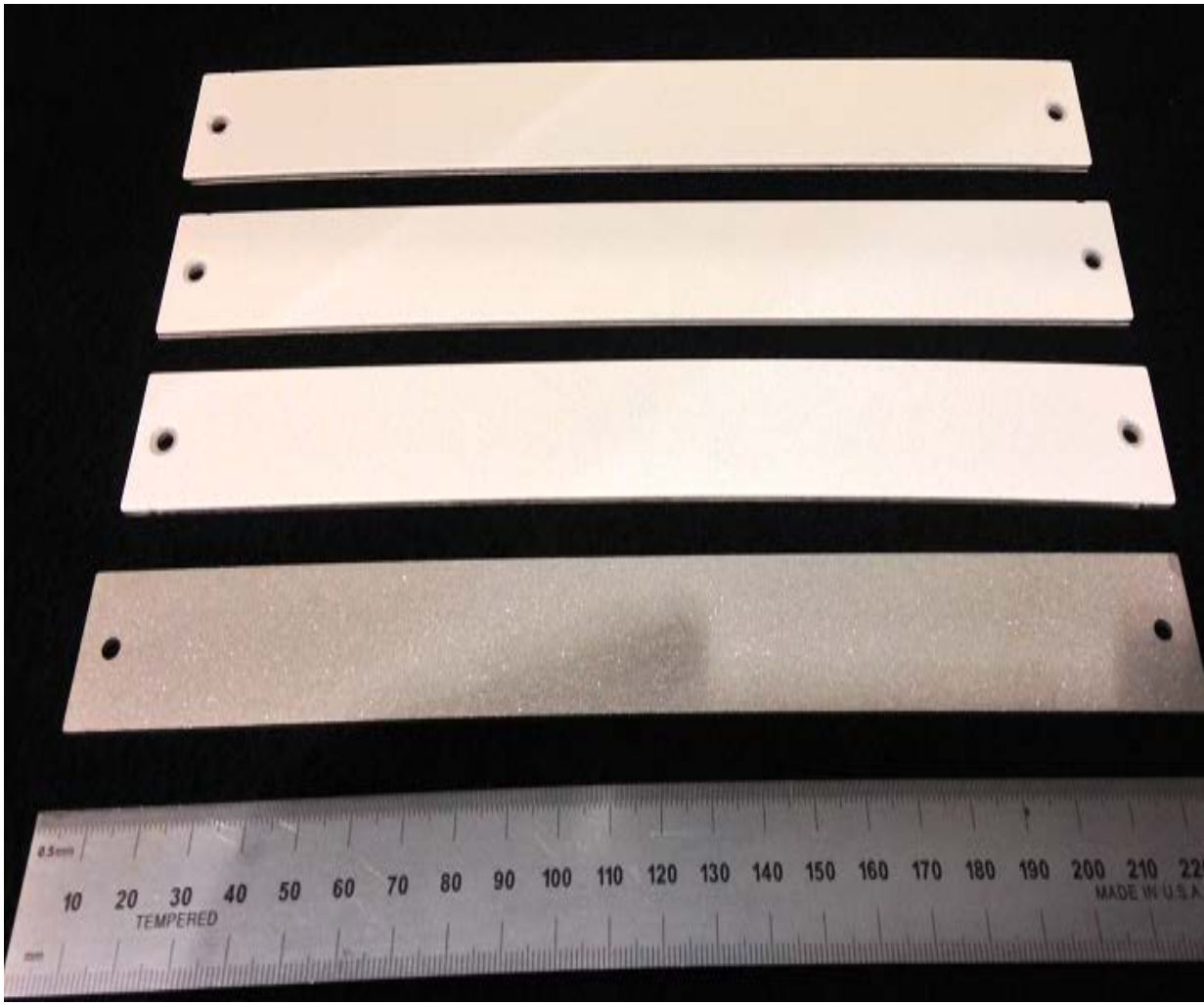

Instrument Layout

Three displacement laser ports directly behind substrate

Two loose pin connections prevent binding as beam curves during deposition run

Subjectivities of ICP

Sample Prep:

- Grit blasting removes surface oxides and introduces surface texture for mechanical adhesion
- Induces offset curvature that will offset the curvature caused by the coating stresses

Solution:

- Automate grit blasting process (costly)
- Apply to both sides of beam in attempt to “balance” the induced curvature
- Use one operator to perform all grit blasting for a given project

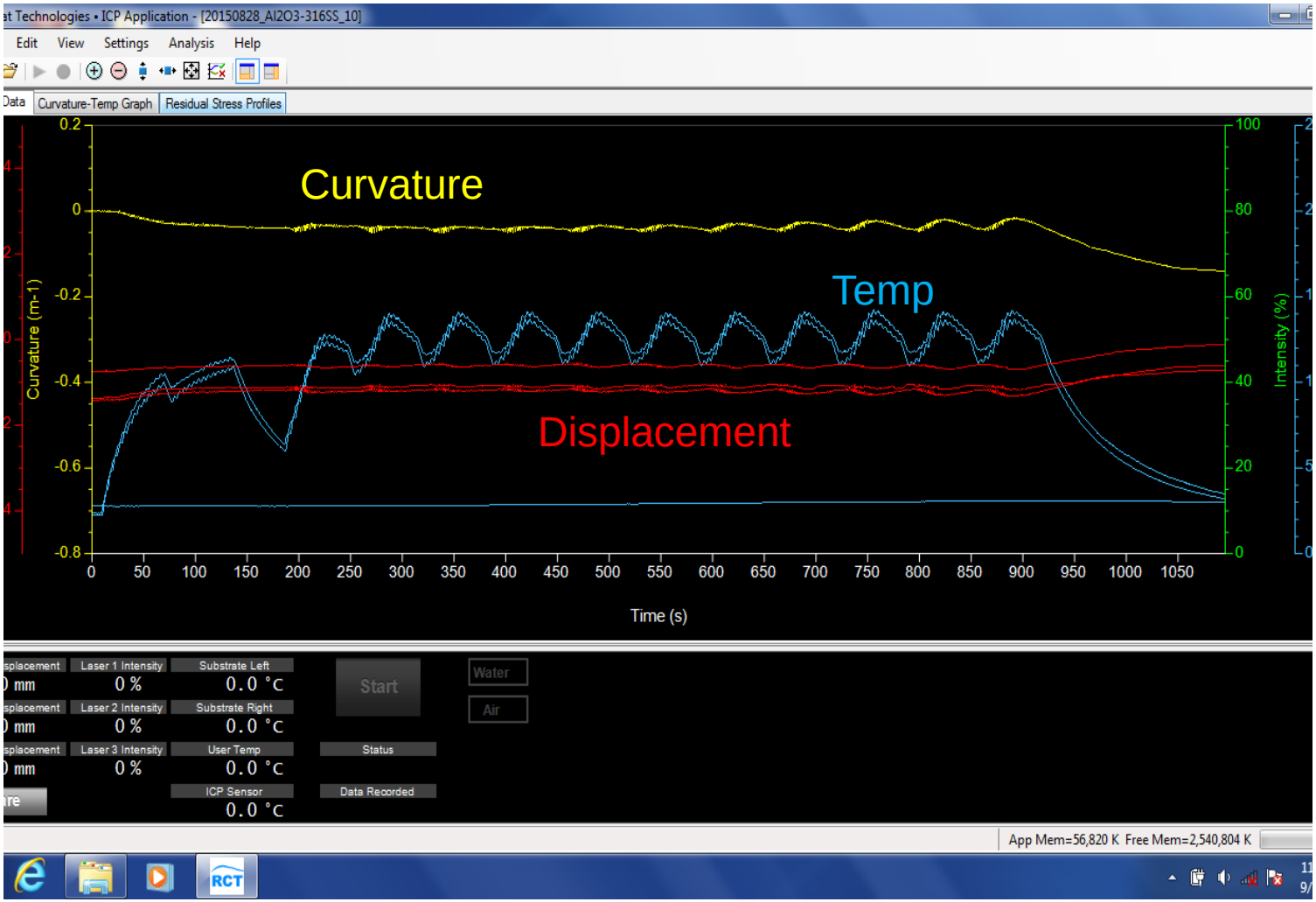

Temp (blue) note pre-heat, steady state through several raster passes

Three lasers (red) two at ends of lesser magnitude than center shows convex bending

Curvature (yellow) shows increasing flex with thermal cycling as spray run progresses, then slowly increases as thermal stress builds on cooling

Real-Time Data Collection Screen

Deposition Stress + Thermal Stress = Residual Stress

Subjectivities of ICP

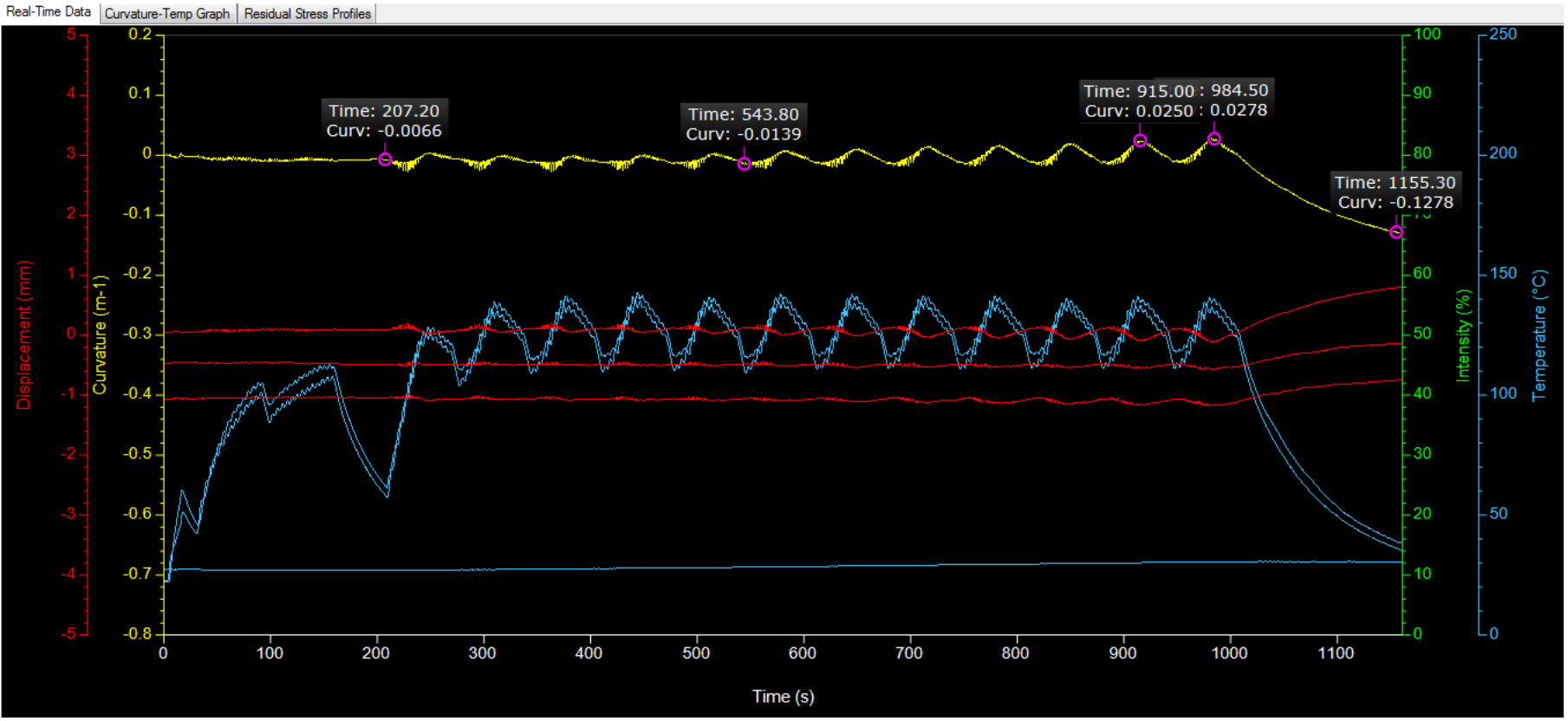

Selection of points performed by operator:

- Beginning and end of spraying
- Beginning and end of deposition stress regime
- End of cooling (approx. room temp)

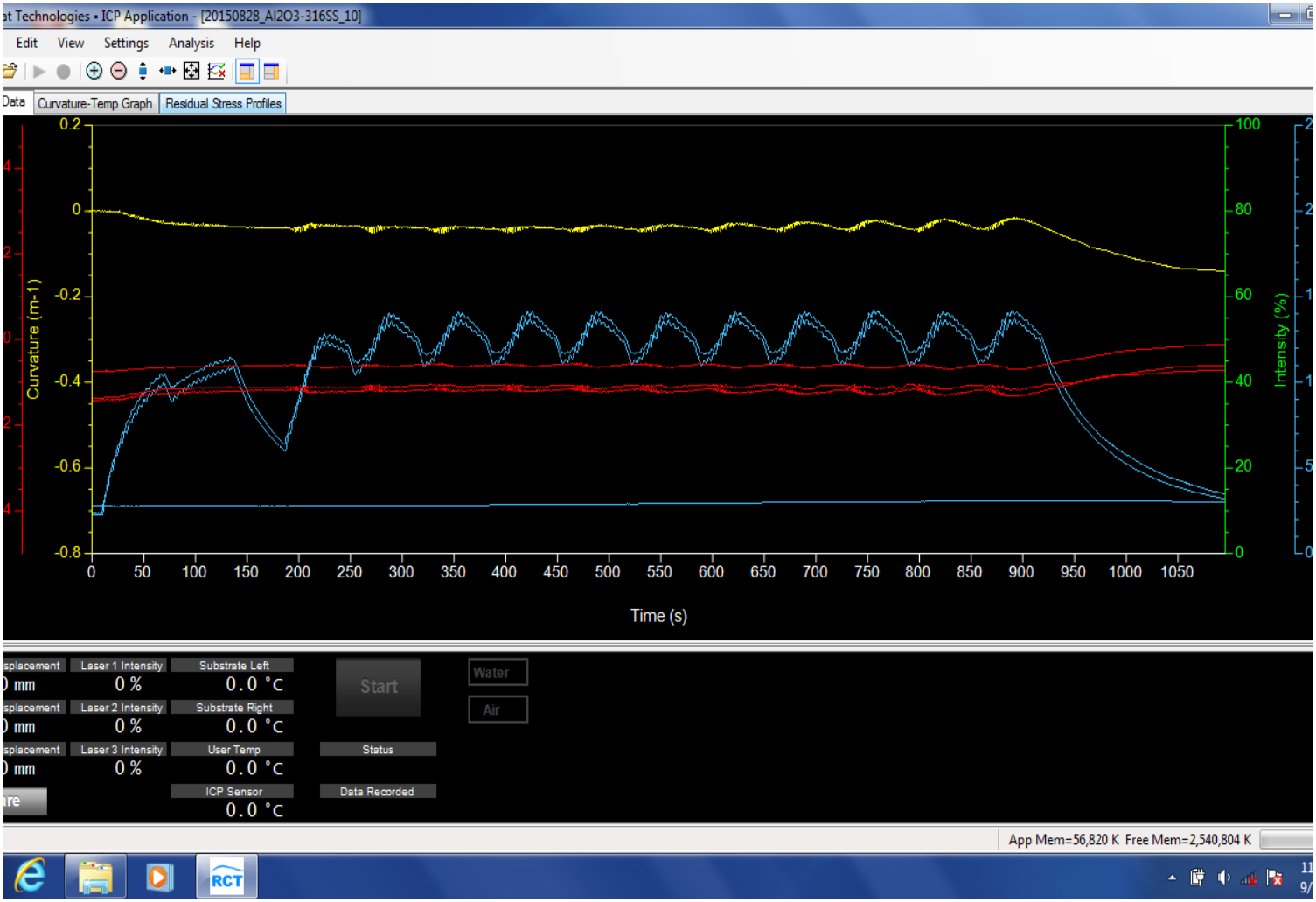

Temp (blue) note pre-heat, steady state through several raster passes

Three lasers (red) two at ends of lesser magnitude than center shows convex bending

Curvature (yellow) shows increasing flex with thermal cycling as spray run progresses, then slowly increases as thermal stress builds on cooling

Real-Time Data Collection Screen

Stress Profile Plot

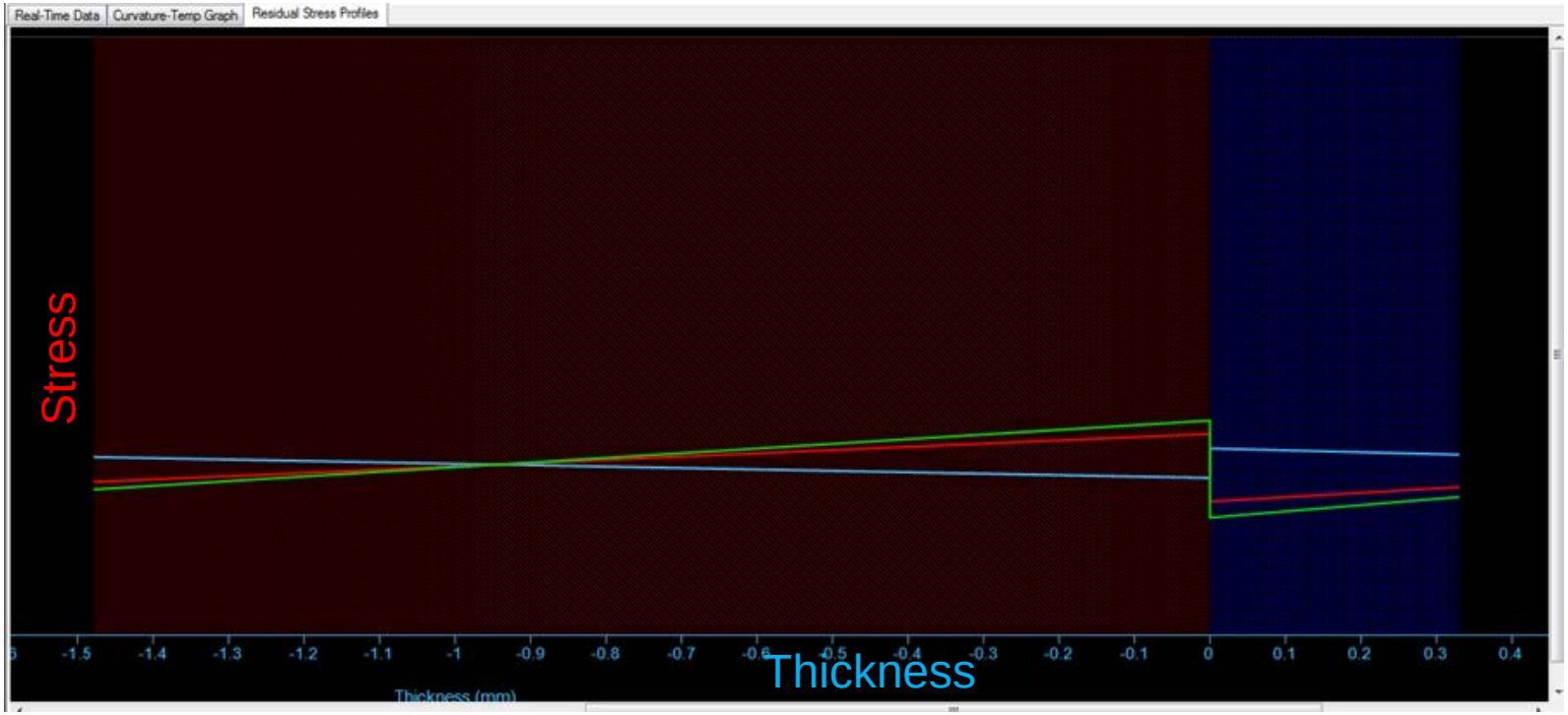

Stress profile shows build of stress through thickness of substrate and coating

Note differing slope of deposition stress (blue) and thermal stress (red)

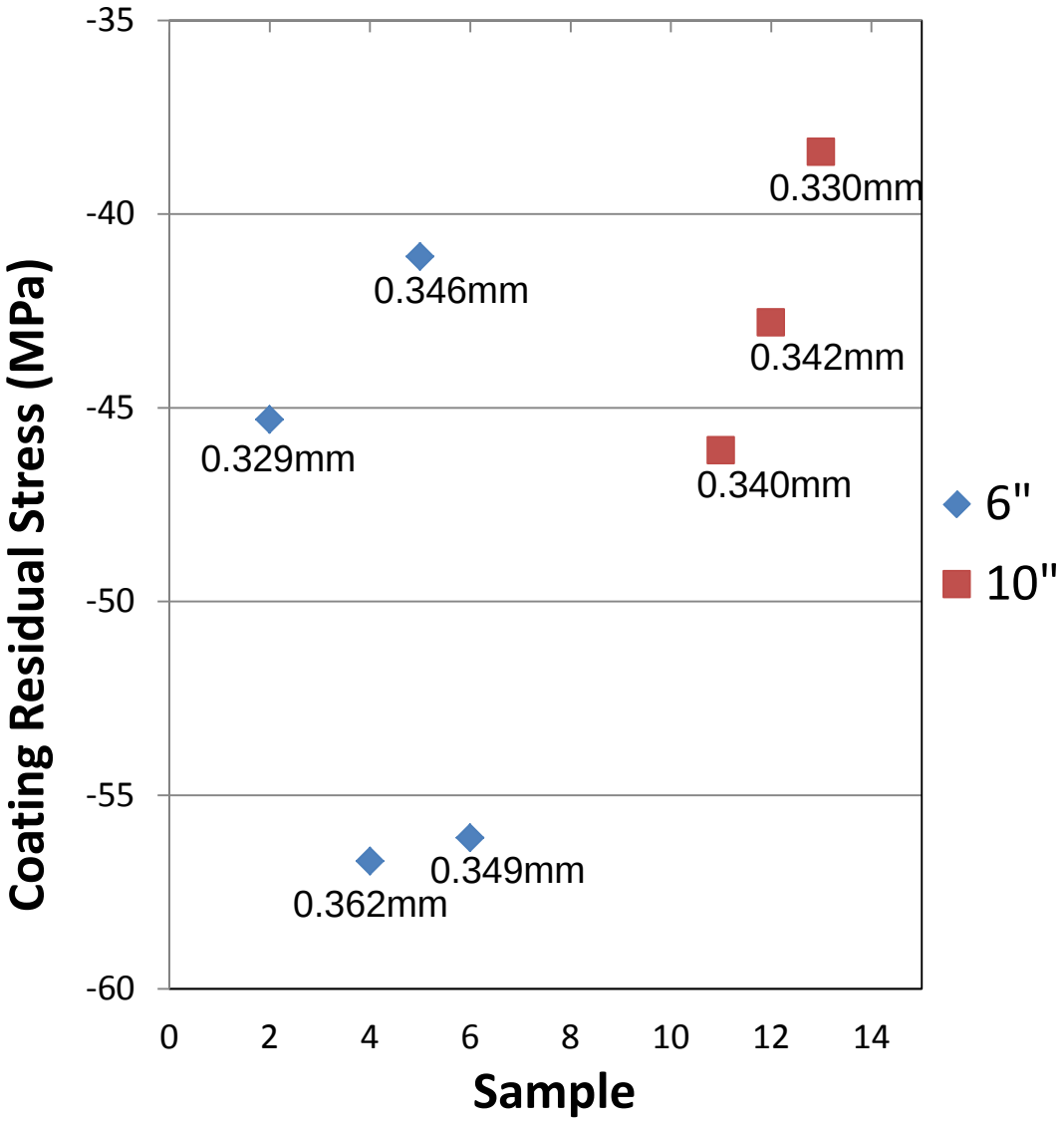

Residual Stress = Quenching Stress + Thermal Stress

Large variability due to process variation

Reproducibility of process measured by variability of residual stress

Elastic modulus determined for linear range selected from Curvature – Temp plot.

Compare to bulk alumina modulus ~ 300 GPa. [accuratus.com]

Large variability due to process variation

Reproducibility of process indicated by variation of coating modulus

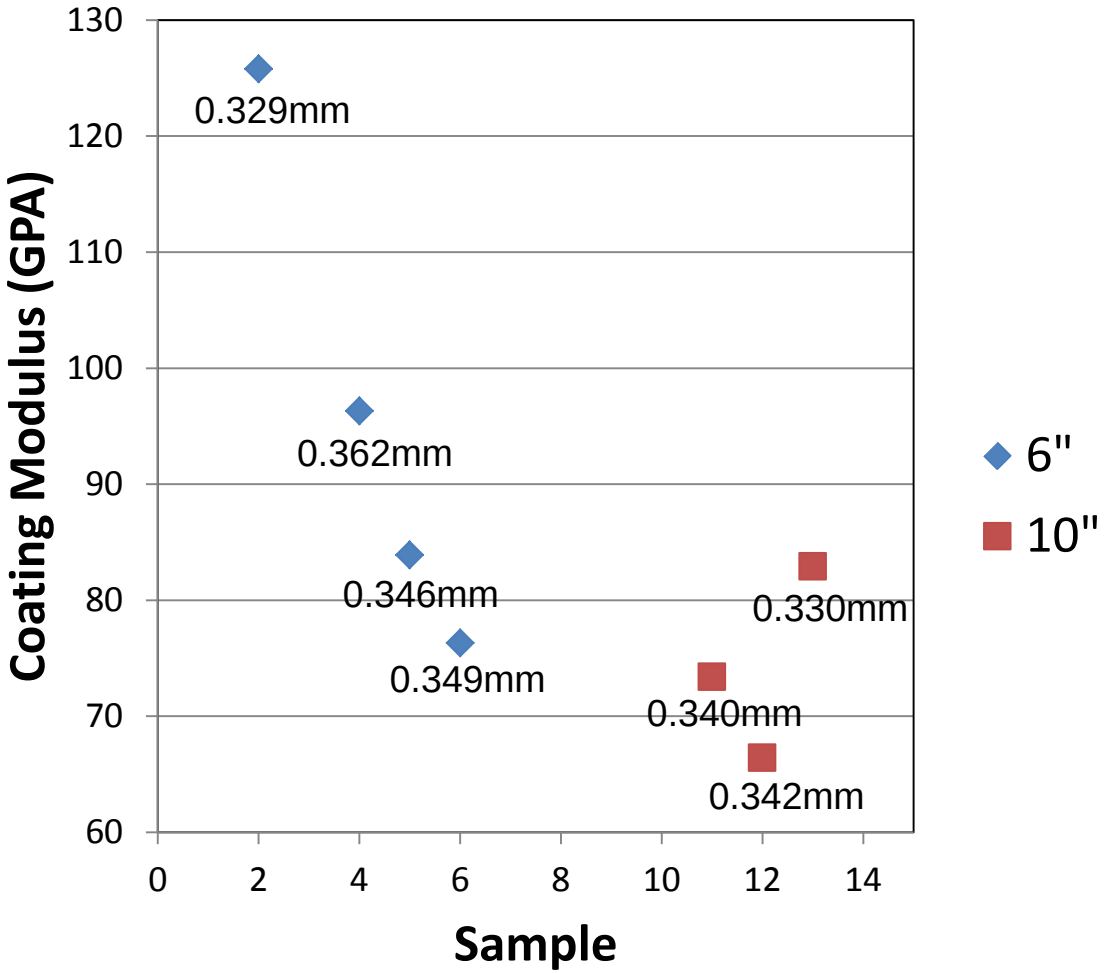

ICP Data & Clyne Equation

$$\Delta\kappa = \frac{6E_0E_S(h+H)hH\Delta\alpha\Delta T}{E_D^2h^4 + 4E_DE_Sh^3H + 6E_DE_Sh^2H^2 + 4E_DE_ShH^3 + E_S^2H^4}$$

$$\Delta\kappa \propto \frac{hH\ \Delta T}{(h+H)^3}$$

Input

- $E_{substrate}$
- $E_{coating\ (bulk)}$
- Substrate Thickness (H)
- Coating Thickness (h)
- Coating Weight
- Feedstock Flow Rate
- Traverse Speed

Output

- $E_{substrate}$ (calculated)
- $E_{coating}$ (calculated)
- Curvature (K)
- ΔT
- Deposition Efficiency

Six inch standoff

Ten inch standoff

Sandia National Laboratories

zoom

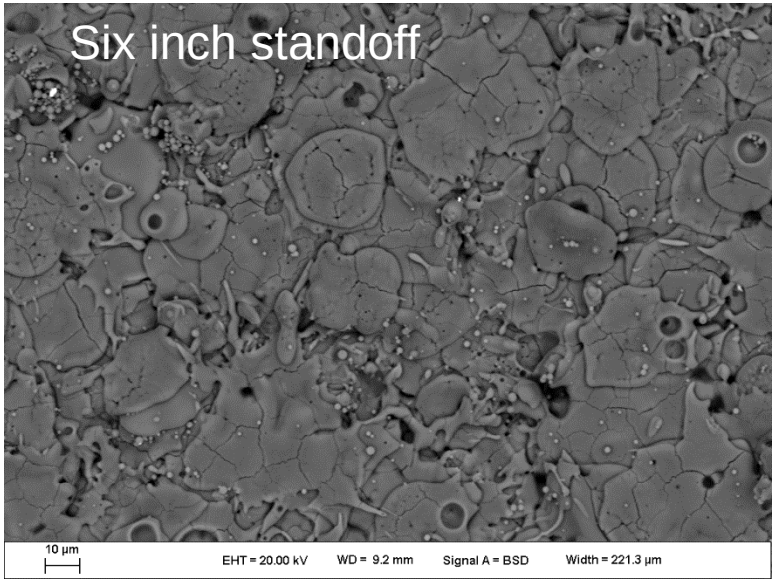

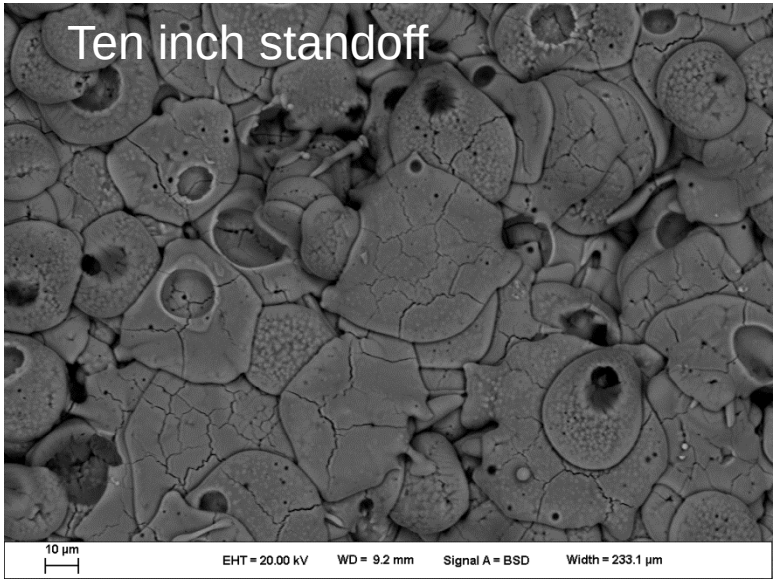

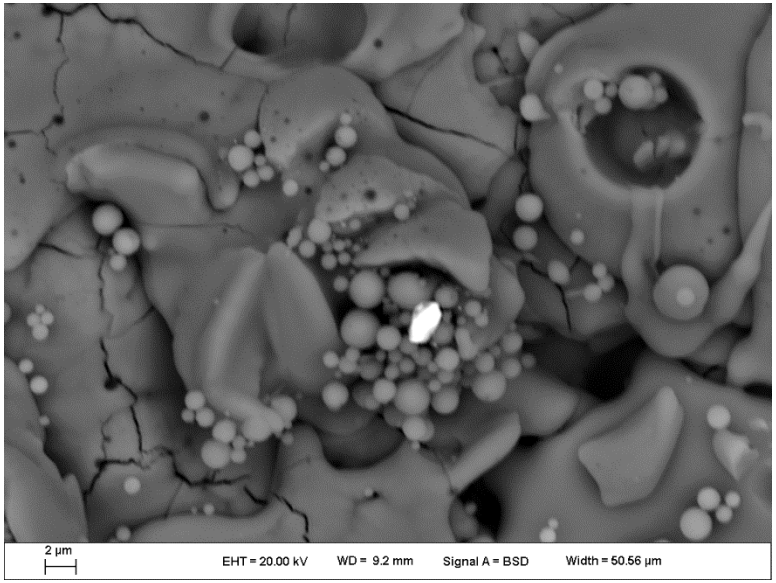

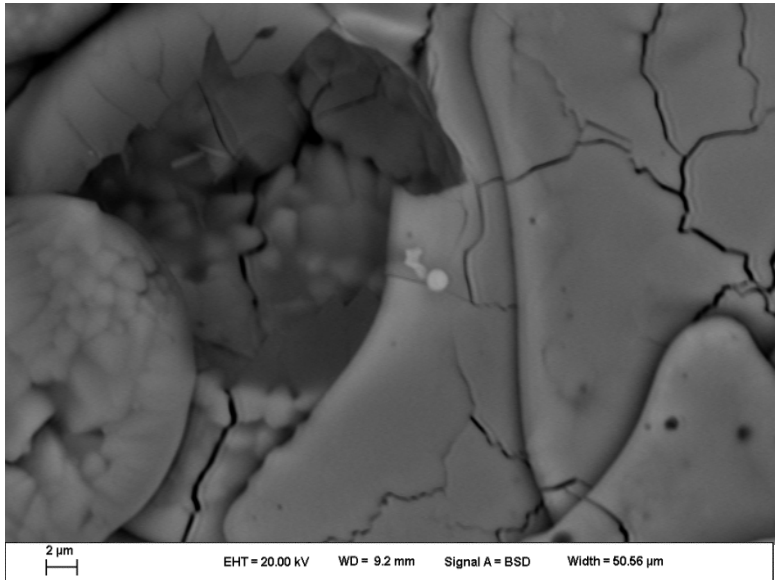

Smaller splat diameters. More splashing.
Less craters.
More fine spherical particles (not splats).

Larger splat diameters. No splashing.
More and larger craters.
Dendritic solidification?

Conclusions

TSRL currently has capacity to capture relevant process parameters and variations.

TSRL now has instrumentation to measure coating product properties in-situ, at the point of production

For this particular experiment, 6” standoff yielded particles with higher velocity and temperatures, resulting in coatings with higher magnitude of compressive residual stress and higher modulus.

Future work will focus on tuning these input and output parameters to determine repeatability of sprayed coatings for increased efficiency and higher quality products

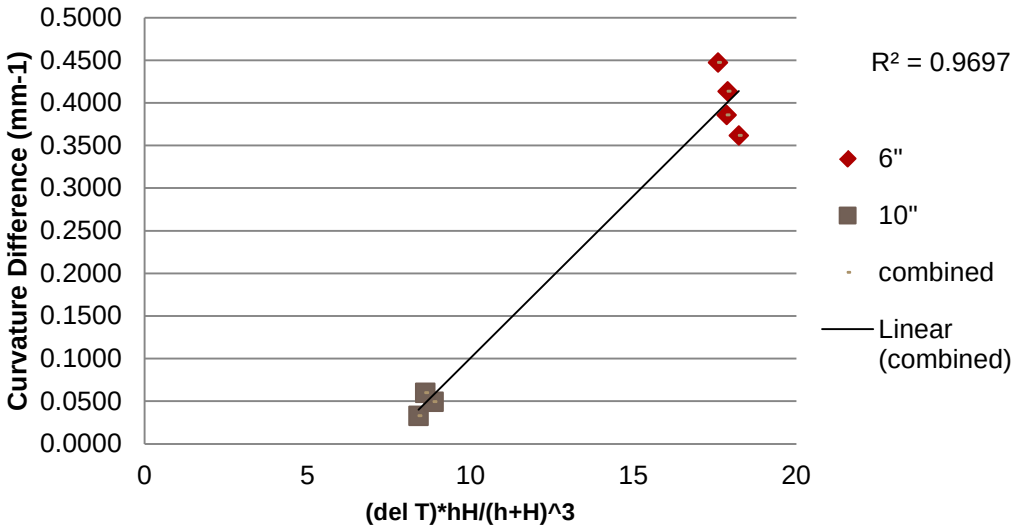

$$\Delta\kappa \propto \frac{hH\ \Delta T}{(h+H)^3}$$

Sandia National Laboratories

Deformation of Alumina Particles in Compression –
Basis for a Room Temperature Ceramic Coating Deposition

AEROSOL DEPOSITION

Motivation

Aerosol Deposition (AD) enables materials integration.

- Ceramics are conventionally processed at 2000°C.
- AD process at room temperature (RT) in vacuum
  - sub-micron particles accelerated to high velocity by pressurized gas, impacted, consolidated to form a film.
- Similar AD ceramic film microstructures
  - sub-micron particles undergo *plastic deformation*
  - break up into *small crystallites* (20-75 nm)[1-3]
  - planar *defects* and *amorphous regions*[4].

Particle deformation/bonding not well understood

- Common deformation mechanisms exist.
- Examine sub-micron ceramic particles RT deformation as a building block for AD coatings.

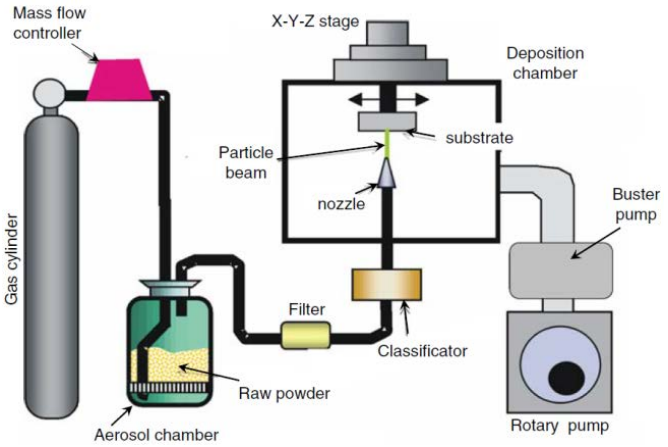

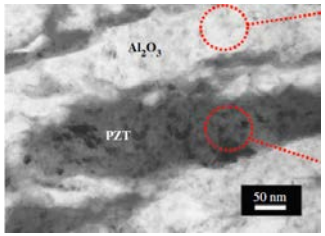

AD process and coatings from Akedo *J. Am. Ceram. Soc.*, 2006;89:1834

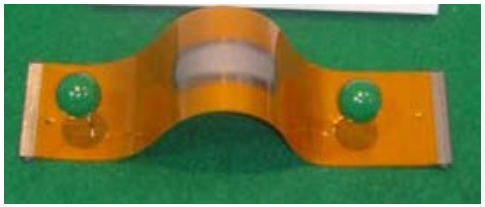

AD Flexible electronics from J. Akedo. *JTTEE5.,* 2007:17:181

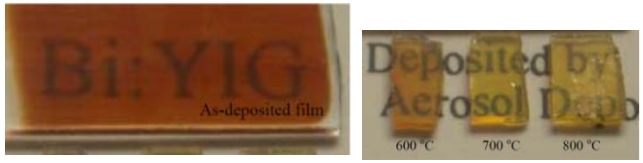

AD magnetic films from Mizoguchi et al. J. Magnetic Soc Japan 2006:30;659

[1] Akedo, J. and Ogiso, H., *JTST*, Vol. 17, (2008), pp. 181-198.
[2] Akedo, J., *JTTEE5*, Vol. 17, (2007), pp. 181-198.
[3] Akedo, J. *J. Am. Ceram. Soc.*, Vol. 89, (2006), pp. 1834-1839.
[4] Park, H. *et al*. Scripta Materialia, 2015.

Motivation

AD Deposition efficiencies are low

Why do some ceramic particles deform and others don't?

Akedo presented data indicating an optimum milling time but no explanation. Why is milling important?

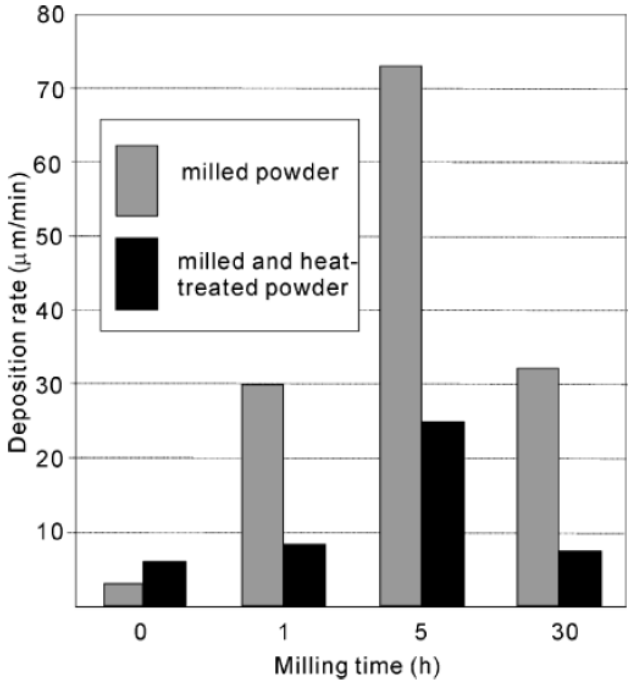

Fig. 4. Deposition rate for PZT film formation at room temperature using powder milled for different duration times with (black bar)/without (gray bar) heat-treatment procedure at 800°C for 4 h in air. The deposition area is 5 × 5 mm^2.

Akedo & Lebedev, Jpn. J. Appl. Phys. V. 41(2002) 6980-4

Motivation

- Bulk materials with high degrees of covalent/ionic bonding, e.g. ceramics, typically undergo brittle fracture when strained.
  - a combination of limited fracture toughness and preexisting flaws.
  - The role of pre-existing flaws and defects can evolve as the characteristic length scale of materials decrease (e.g. micro-pillars and particles) [1-14].
  - In bulk ceramics →crack initiation sites.
- **At small length scales, significant plasticity observed in ceramic single crystals at room temperatures.**
  - Low strain rates → dislocation slip and shape change
    - compressed sapphire micro-pillars [10], particles [16], and confined zones underneath an indenter [36] at RT.
  - High strain rates → aerosol deposition (AD)
    - < 2 μm particles are accelerated to high velocity (200-600 m/s) by pressurized gas, impacted, deformed, and consolidated on the substrates under vacuum [16-24].
- Room temperature plasticity in ceramics at small length scale gave insights into future development of alternative ceramic forming technology and high strength/high toughness functional ceramics.
- The focus of this study is to better understand the deformation behavior observed in small-scale, compressed ceramic particles, specifically sapphire or α-Al_2O_3 and how they play a role in making AD coatings.

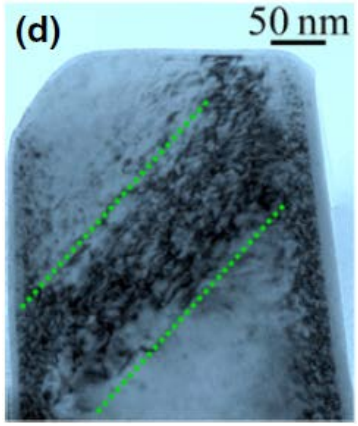

Dislocations on {001} planes in compressed ZrC pillar from S. Kiani, *et al. J. Am. Ceram. Soc.*, 2015:98:2313

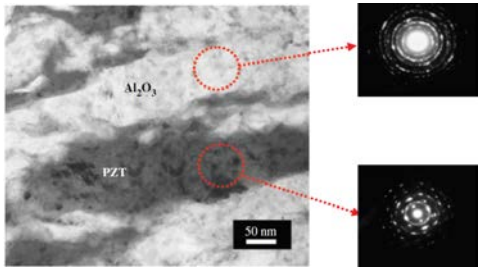

AD Al2O3 and PZT composite film from J. Akedo. *J. Am. Ceram. Soc.*, 2006:89:1834

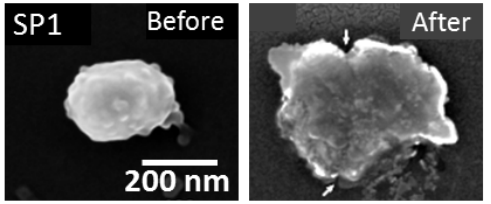

Compressed sapphire particle from P. Sarobol, *et al.*, *JTST.*, 2016:25

Previous work – P. Sarobol, et al., *JTST*., 2016:**25**

DOI 10.1007/s11666-015-0295-2

Sandia National Laboratories

- Performed micro-compression on 3.0 µm and 0.3 µm Al_2O_3 particles
- Micron sized particles - brittle fracture
  - Absorbed strain energy density before fracture **107 ± 69 MJ/m³**
  - Strain before fracture **5.5 ± 1%**
- Sub-micron sized particles - substantial plastic deformation before fracture.
  - Absorbed strain energy density before fracture **630 ± 238 MJ/m³**
  - Strain before fracture **18 ± 9 %**
  - Deformable sub-micron sized particles = AD coating building block

- **6x** higher strain energy density
  - dislocation nucleation
- **3x** higher accumulated strain

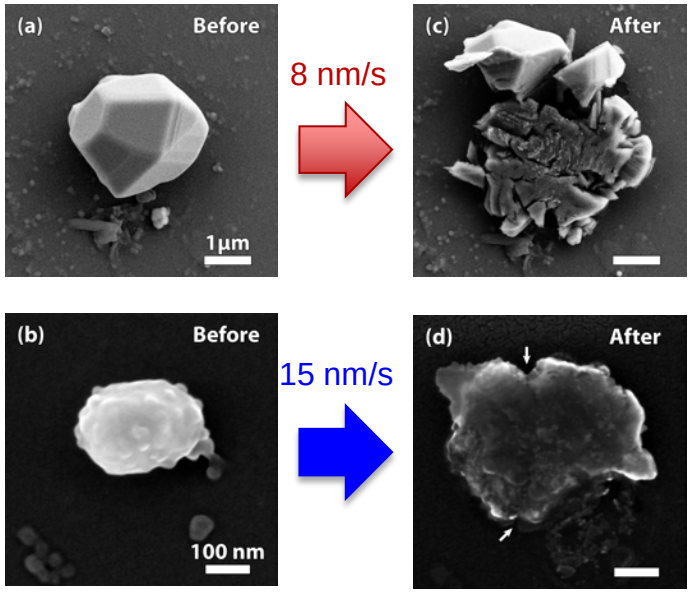

	Micron	Sub-micron
# Pre-existing Defects	High	Moderate
Energy Density Input	Low	Moderate
Governing Mechanism(s)	Fracture	Plasticity + Fracture
Response to Compression	Crack initiation & Propagation	Dislocation nucleation, slip, crack initiation & propagation

Sub-micron sized Al_2O_3 response to compression
– *In Situ* TEM micro-compression
– Molecular Dynamics Simulation

In Situ TEM Compression

Sandia National Laboratories

In Situ Micro-Compression[5] – 300 nm particles

- Single crystal, ultra pure 300 nm sapphire (α-Al_2O_3) particles.
- A Hysitron PI95 TEM Picoindenter with a 1 µm diameter flat punch tip and the a JEOL 2100 LaB_6 TEM[7] at 200 kV were used.
- Compression done in ***open loop*** mode with the loading rate of 10 µN/s (approx. **< 2 nm/s** displ rate). Images taken at 15 fps.

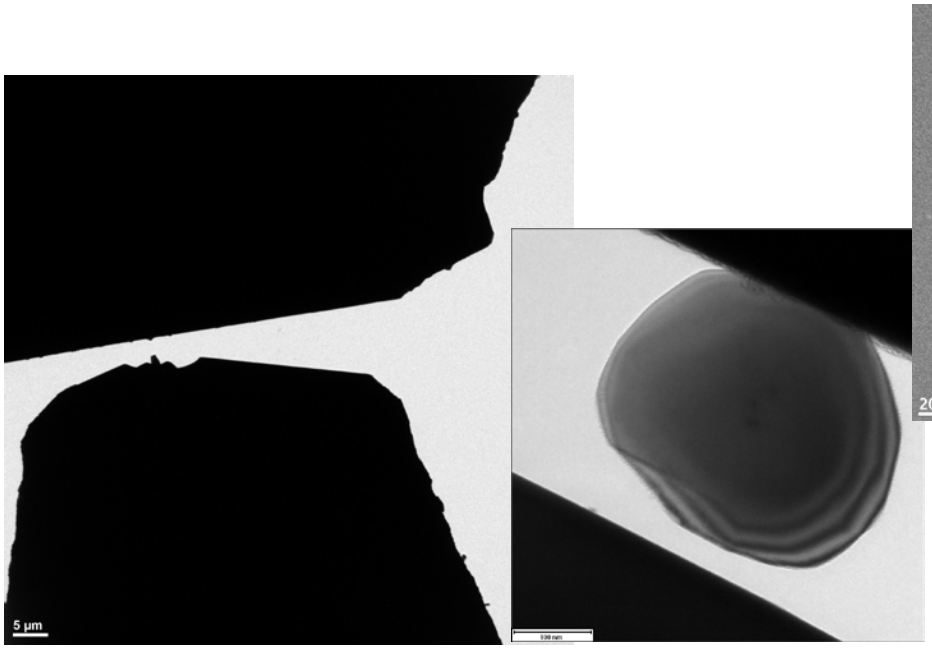

***In situ* TEM micro-compression on 0.3µm particle**

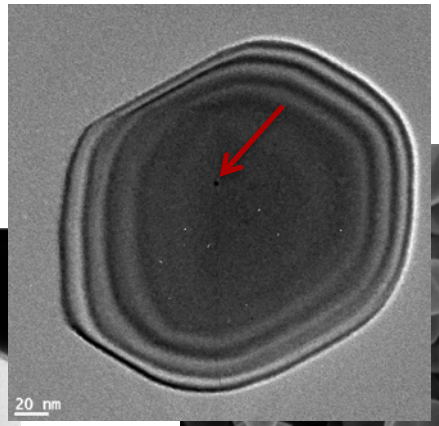

Bright field TEM image of a 300 nm particle oriented on the [001] zone axis.

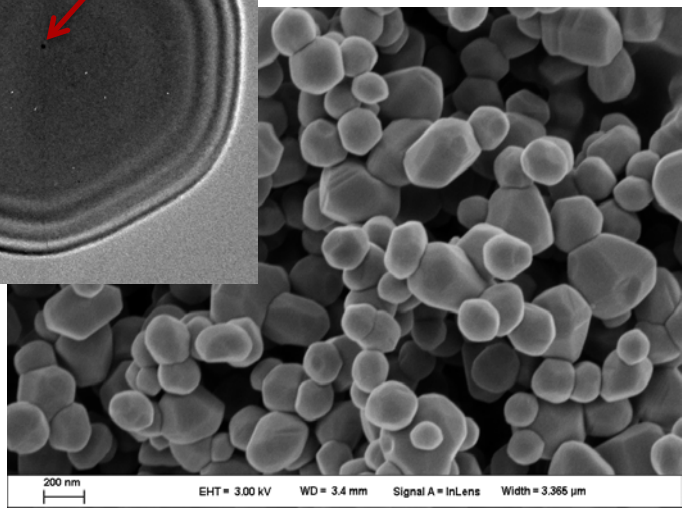

SE SEM image of the 300 nm

[5] Sarobol, P., *et al*., *SAND2014-18127*, (2014).
[6] Hysitron I (2013) SEM Picoindenter User Manual. Revision 9.3.0913 edn.
[7] Hattar, K., et al., Nuclear Instruments and Methods in Physics Research B. Vol. 338, (2014), pp. 56–65.

In Situ TEM Compression

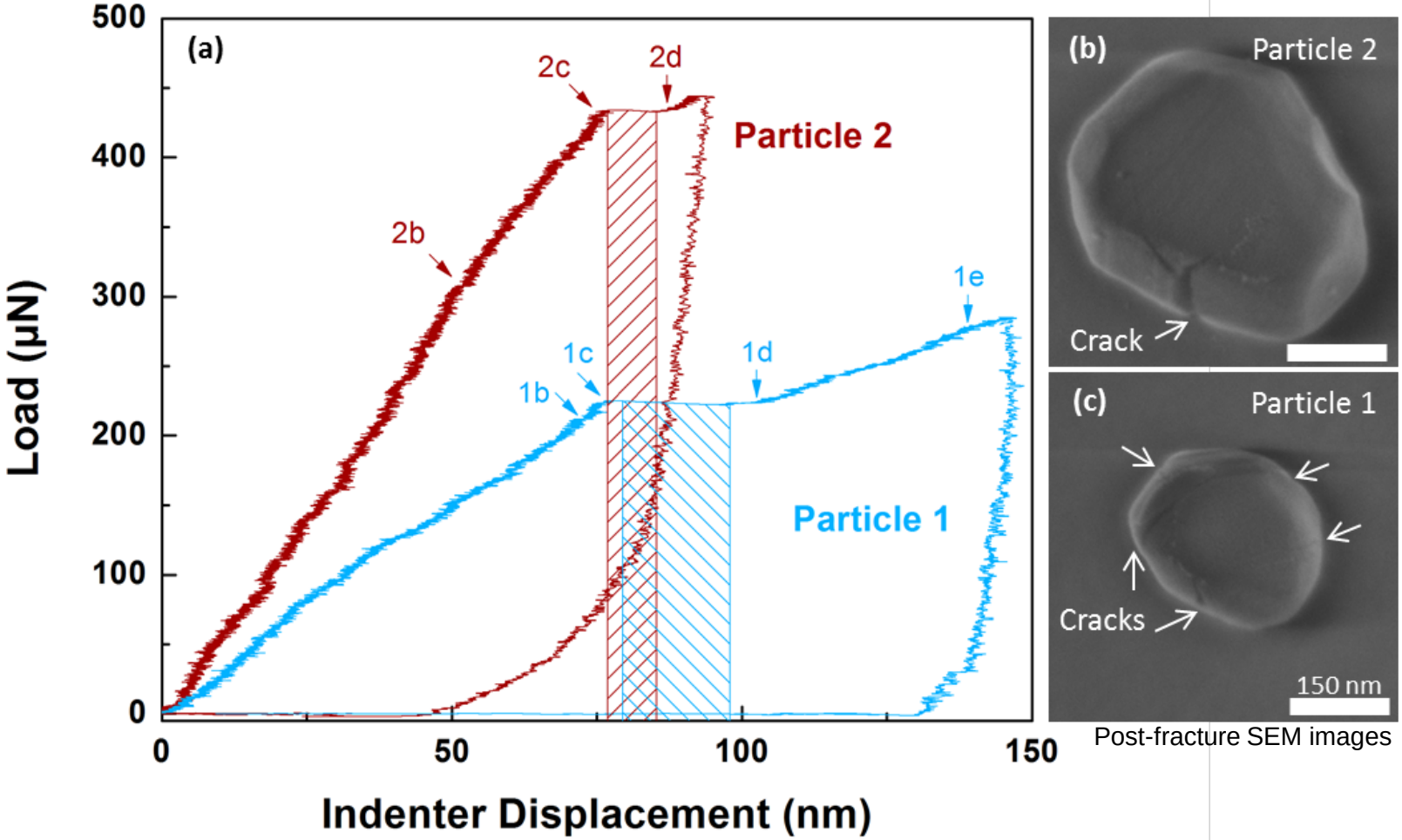

Post-fracture SEM images

- Elastic to Plastic transitions are unclear. Seemed to happen much earlier in the loading (first 5-10 nm displacement). Absence of concavity and linearity of the curves were surprising.
- G_C values for Particle 1 and 2 are 45 J/m^2 and 17 J/m^2, respectively. Values within the calculated range of orientation-dependent G_C of single crystal alumina of 16 - 65 J/m^2 [47].

In Situ TEM Compression – P1

Diameter ~ 0.24 µm, Open loop, Strain rate ~ 0.009 s^{-1}

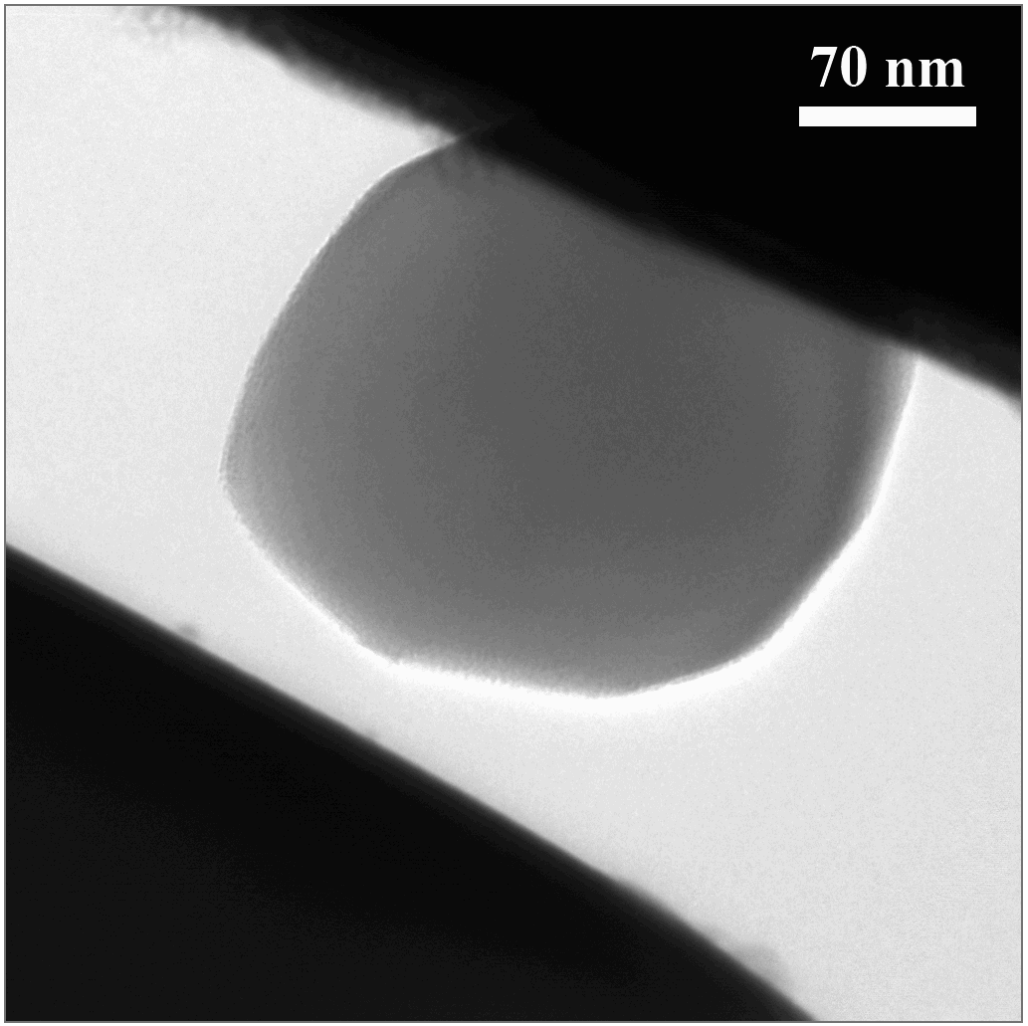

Large displacement gain at a constant load ("burst") corresponds to particle fracture.

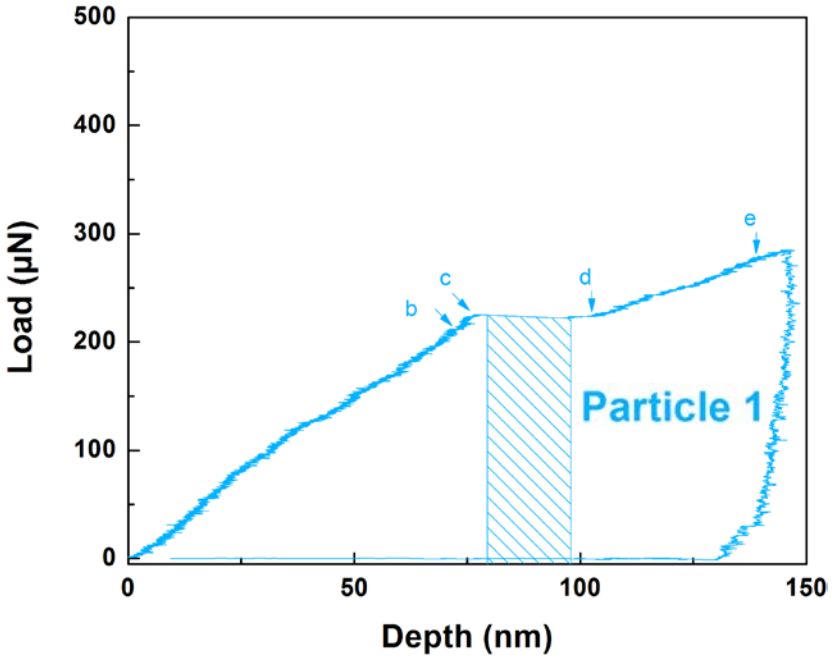

In Situ TEM Compression – P1

Zone axis near $[\bar{9}\,\bar{9}\,18\,6]$

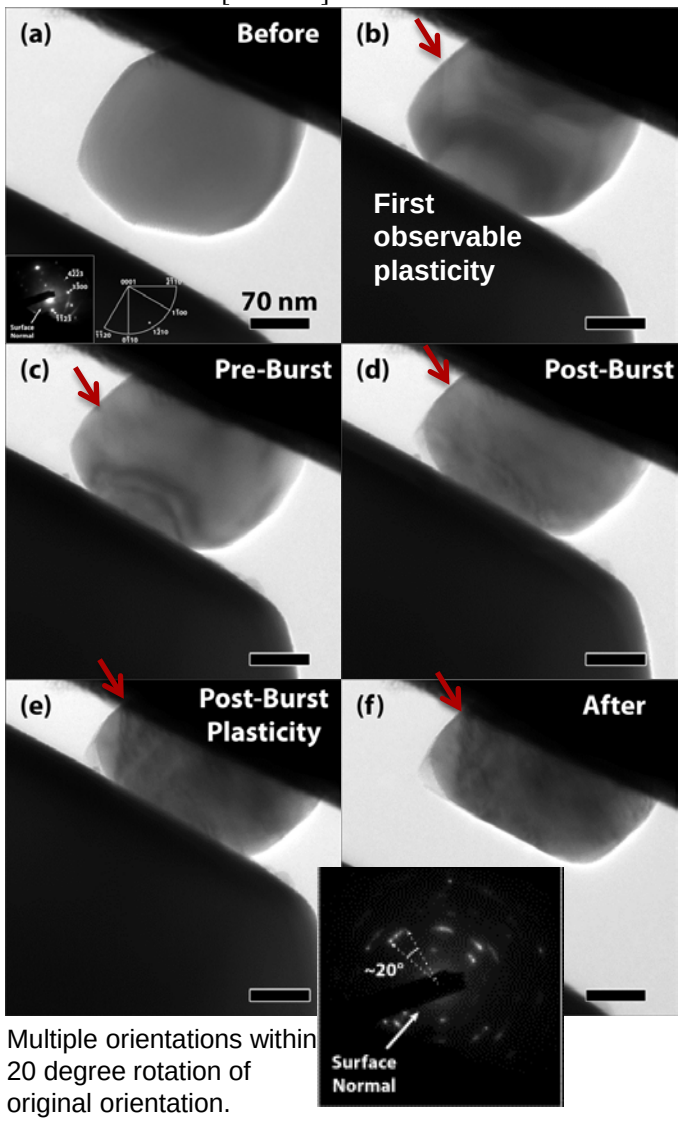

Multiple orientations within 20 degree rotation of original orientation.

- Strain energy release rate = 45 J/m^2

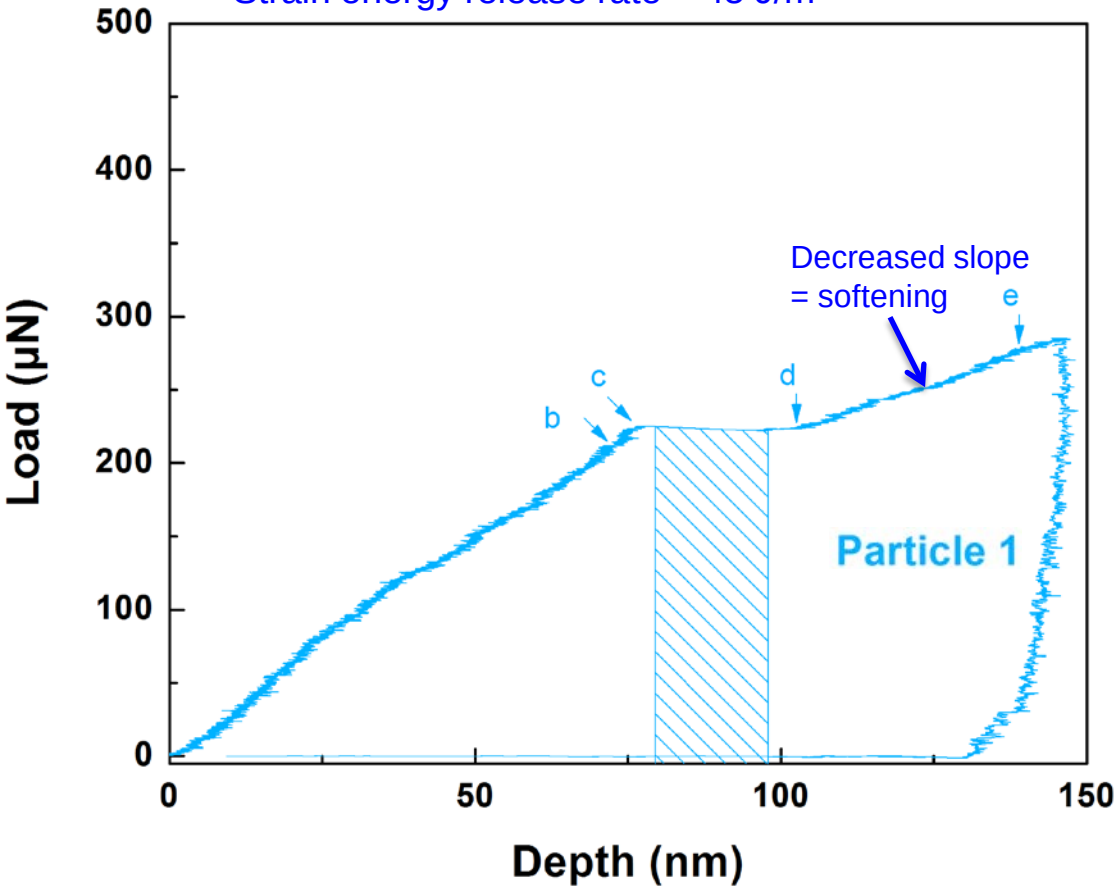

- Pre-burst plasticity: small regime with low dislocation activity.
- **Crack nucleation and propagation** leading to through-particle fracture.
- Post-burst plasticity: high dislocation activities, change in deformation mechanism as indicated by lower slope.
- **Mosaicity** with a 20 degree orientation spread.

In Situ TEM Compression – P2

Diameter ~ 0.38 µm, Open loop, Strain rate ~0.005 s^{-1}

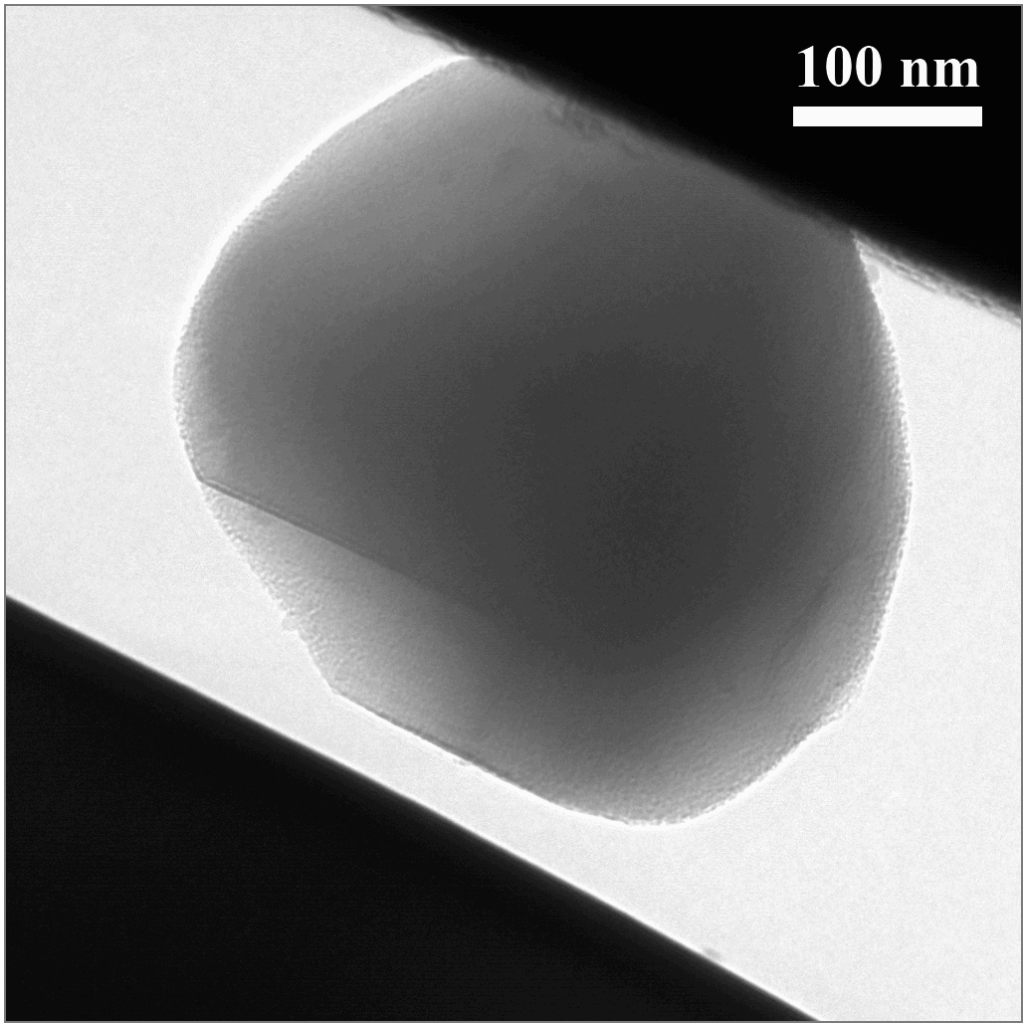

Large displacement gain at a constant load ("burst") corresponds to particle fracture.

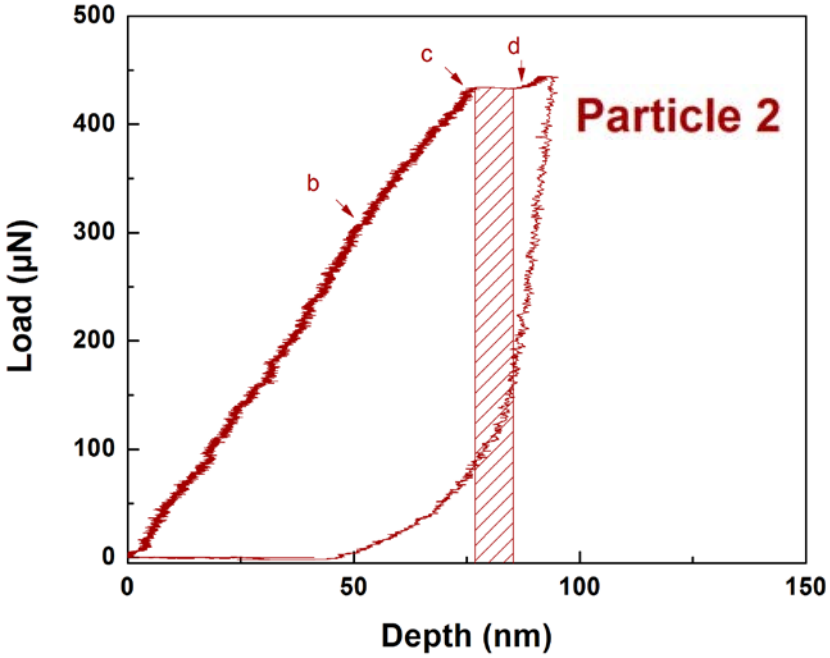

In Situ TEM Compression – P2

Zone axis near $[\bar{2}\ 5\ \bar{3}\ 2]$

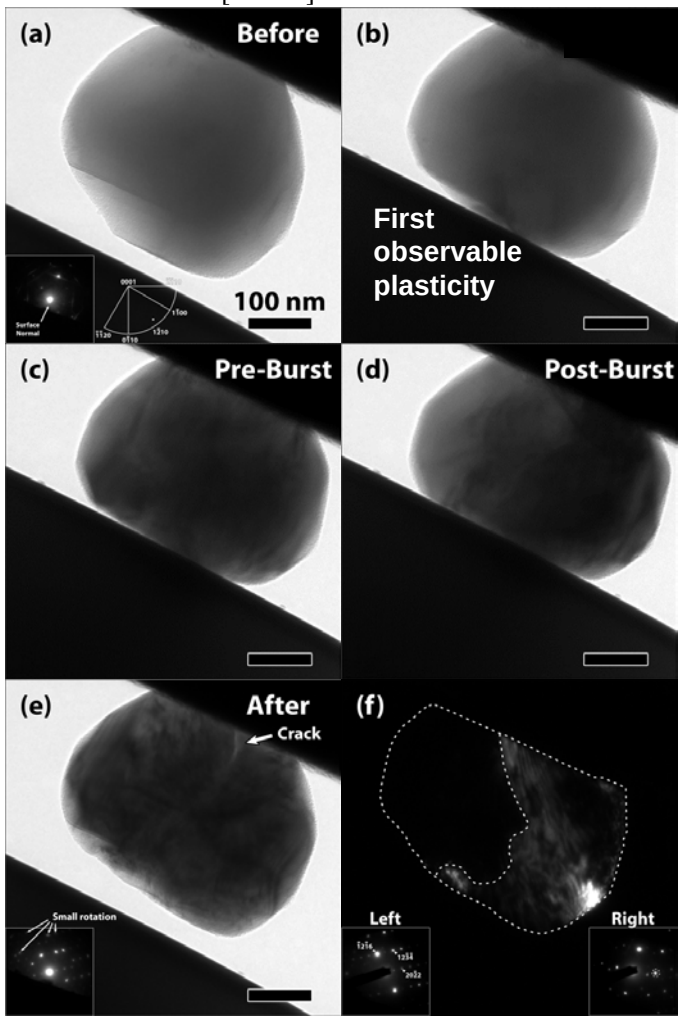

Two halves related by slight rotation, both near $[\bar{1}\ 2\ 1\ 6]$ zone axis

- Strain energy release rate = 17 J/m^2

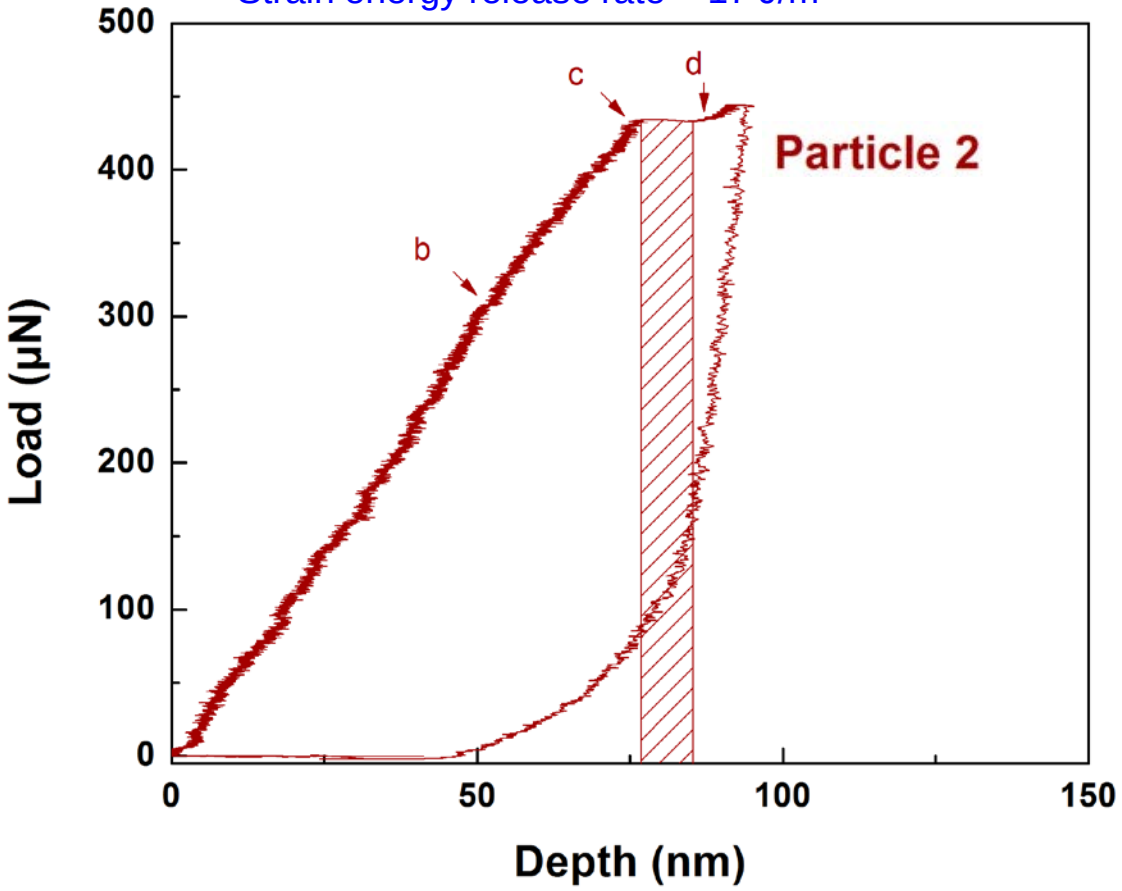

- Pre-burst plasticity: large regime with **high dislocation activity** (nucleation and moving through particle).
- **Crack nucleation and propagation** leading to through-particle fracture.

Simulated Particle Compression

Sandia National Laboratories

Molecular Dynamics Simulations – 10 nm nanoparticles (NPs)

- MD allows identification of dislocations, slip planes, and particle fracture.
- Long computing time to simulate size > 50 nm (~36 million atoms)
- Simulating 10 nm sapphire nanoparticle (NP) (~300,000 atoms)
- A force-field for ceramics, developed by Garofalini[8].
- NPs were compressed (by ~1/3 of the initial diameter) between sapphire (single crystal α-Al_2O_3) walls at a constant velocity of **20 m/s**. **"Displacement control"**.

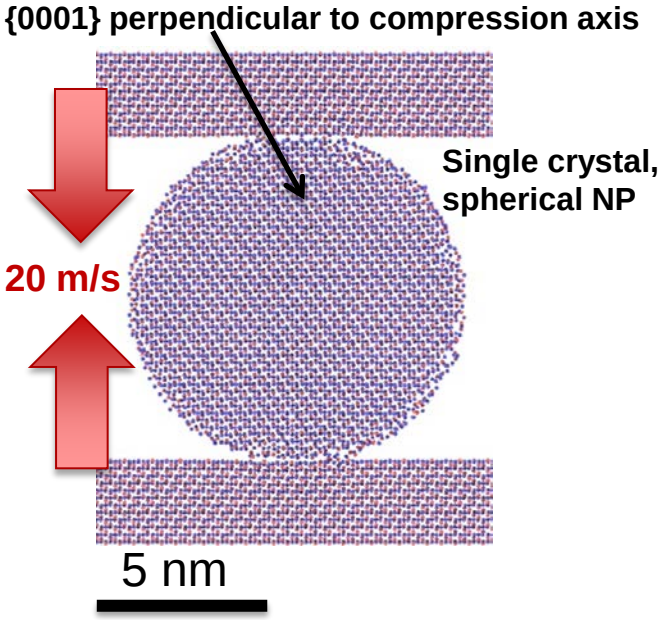

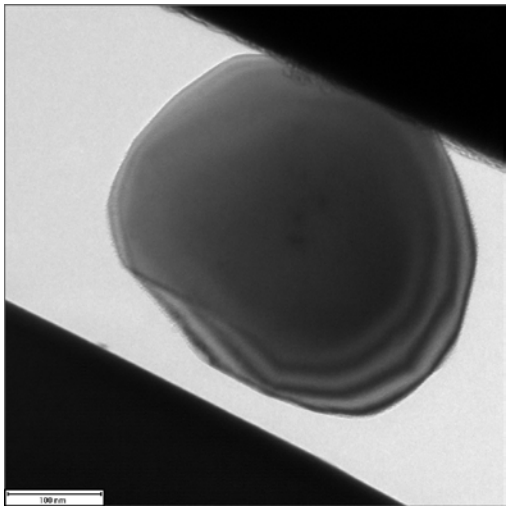

Single crystal, faceted, 300 nm diameter particle

In situ **TEM micro-compression on 0.3μm particle**

[8] Blonski, S. and Garofalini, S. H., *J. Phys. Chem.*, Vol. 100, (1996), pp. 2201-2205.

MD Simulation Results

Sandia National Laboratories

10 nm diameter, defect-free, single crystal α-alumina, compression axis ⊥ (0001)
20 m/s → dislocation nucleation and glide on Rhombohedral planes then fracture

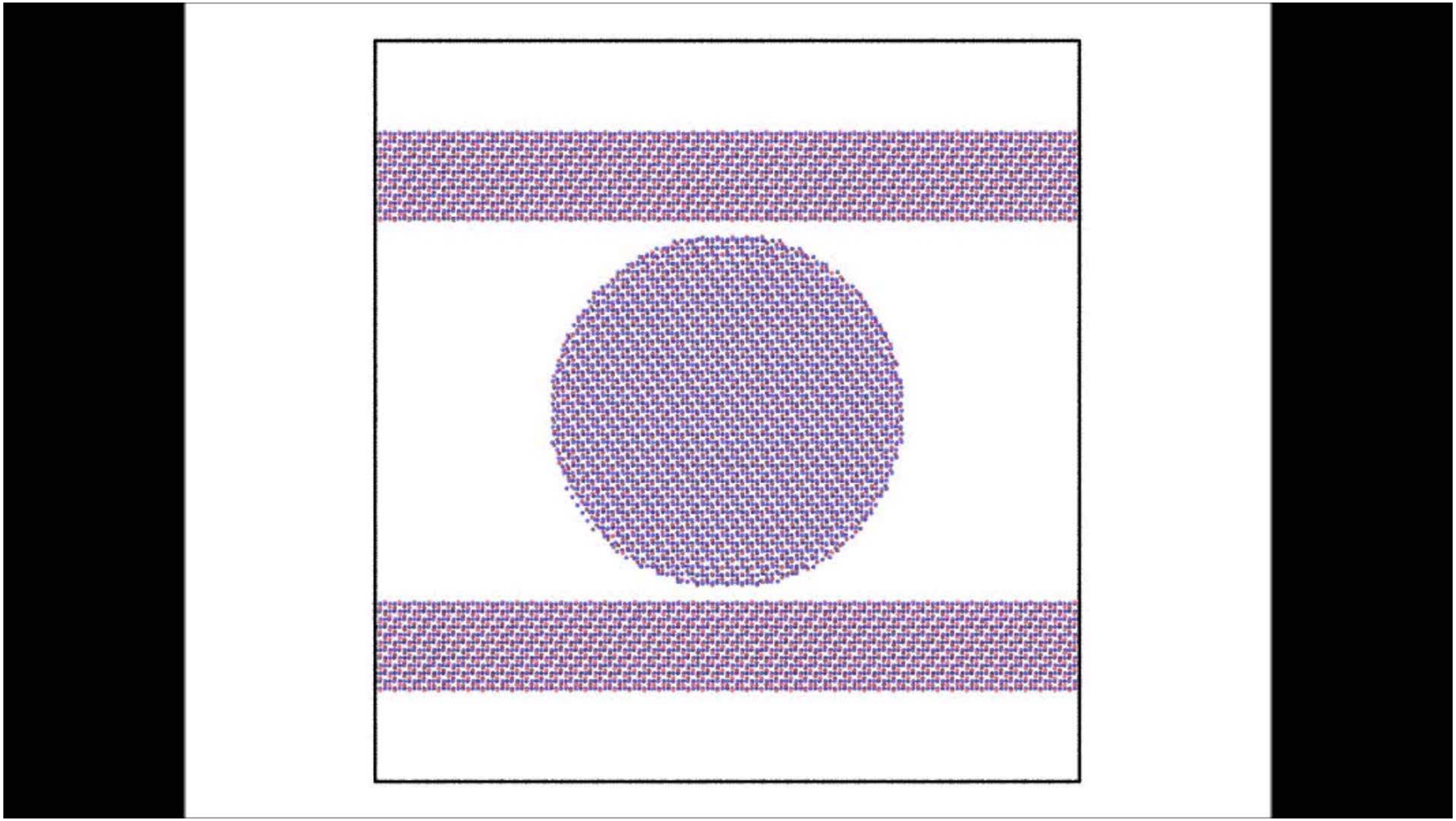

MD Simulation Results

Dislocation plasticity precedes fracture.

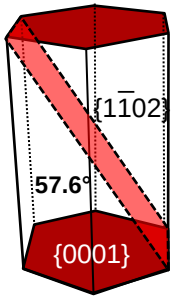

Primary dislocations nucleate at contact points. Then, move through particle on rhombohedral planes

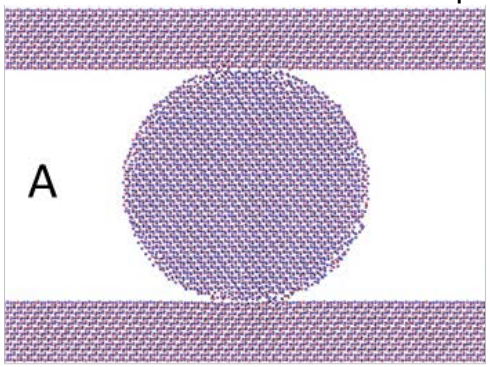

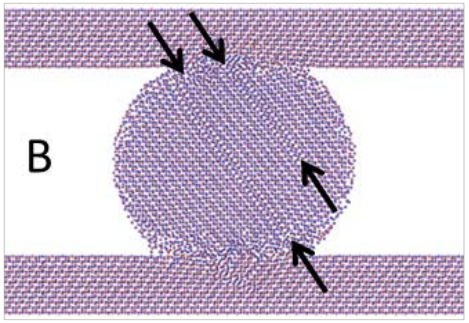

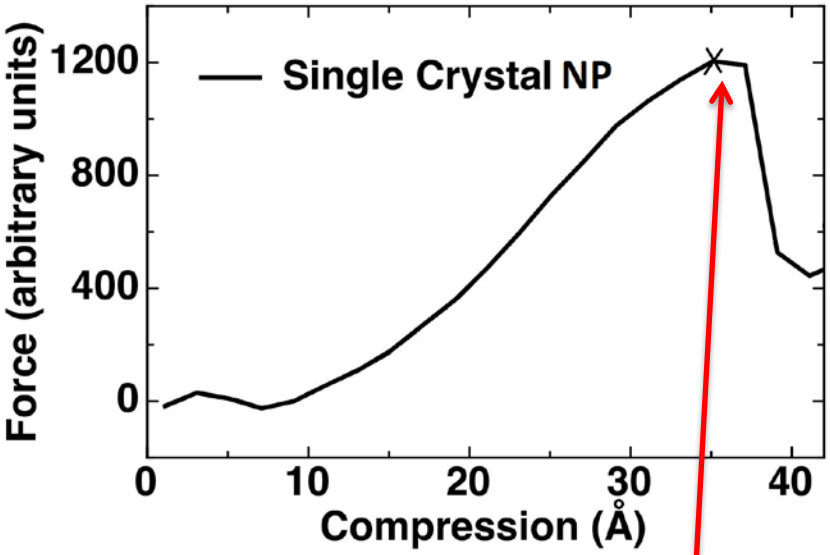

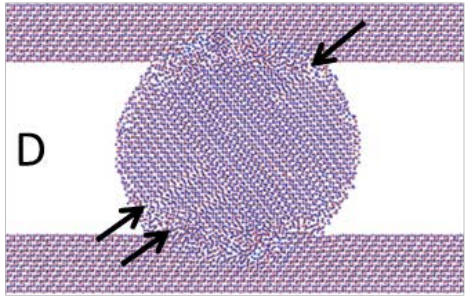

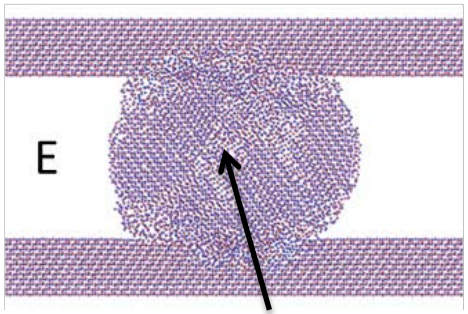

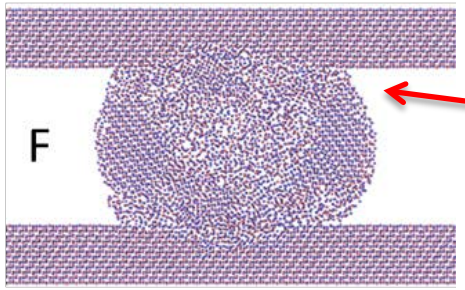

Force drop corresponds to particle fracture

Secondary dislocations nucleate and move through particle on rhombohedral planes, terminating at the primary dislocation planes

Void Initiation

Fracture

Conclusions

- The findings from *in situ* TEM micro-compression experiments and molecular dynamic simulations agree well:
  - Dislocation plasticity precedes fracture in compressed small sapphire particles at RT.
  - Range of responses to compression includes
    - Dislocation nucleation, slip, movement
    - Significant shape change
    - Orientation spread (mosaicity)
    - Fracture
- Use info to inform feedstock preparation, aerosol deposition parameters, and particle-particle bonding in the consolidated coatings.
- Room temperature plasticity in ceramics at small length scale gave insights into future development of alternative ceramic forming technology and high strength/high toughness functional ceramics.

References

1A.R. Beaber, J.D. Nowak, O. Ugurlu, W.M. Mook, S.L. Girshick, R. Ballarini, W.W. Gerberich, *Philos. Mag.*, **91**, 1179 (2011).
2W.W. Gerberich, J. Michler, W.M. Mook, R. Ghisleni, F. Östlund, D.D. Stauffer, and R. Ballarini, *J. Mater. Res.*, **24**, 898 (2009).
3W.W. Gerberich, W.M. Mook, M.J. Cordill, C.B. Carter, C.R. Perrey, J.V. Heberlein, and S.L. Girshick, *Int J Plasticity*., **21**, 2391 (2005).
4F. Östlund, K. Rzepiejewska-Malyska, K. Leifer, L.M. Hale, Y. Tang, R. Ballarini, W.W. Gerberich, and J. Mitchler, *Adv. Funct. Mater*., **19**, 2439 (2009).
5G. Xu and C. Zhang, *J. Mech. Phys. Solids*, **51**, 1371 (2003).
6P.R. Howie, S. Korte, and W.J. Clegg, *J. Mater. Res.*, **27**, 141 (2012).
7W.M. Mook, C. Niederberger, M. Bechelany, L. Phillippe, and J. Michler, *Nanotechnology*, **21**, 05570 (2010).
8H. Bei, S. Shim, G.M. Pharr, and E.P. George, *Acta Mater*., **56**, 4762 (2008).
9F. Östlund, P.R. Howie, R. Ghisleni, S. Korte, K. Leifer, W.J. Clegg, and J. Michler, *Philos. Mag*. **91**, 1190 (2011).
10S. Montagne, S. Pathak, X. Maeder, and J. Michler, *Ceram Int*. **40**, 2083 (2014).
11M.D. Uchic, D.M. Dimiduk, J.M. Florando, and W.D. Nix, *Science*, **305**, 986 (2004).
12D.M. Dimiduk, M.D. Uchic, and T.A. Parthasarathy, *Acta Mater*., **53**, 4065 (2005).
13J.R. Greer, W.C. Oliver, and W. Nix, *Acta Mater.*, **53**, 1821 (2005).
14O.A. Ruano, J. Wadsworth, and O.D. Sherby, *Acta Mater*. **51**, 3617 (2003).
15A. Dominguez-Rodriguez, F. Gutierrez-Mora, M. Jimenez-Melendo, J.L. Routbort, and R. Chaim, *Mater. Sci. Engr. A*. **302**, 154 (2001).
16J. Akedo and H. Ogiso, *JTST*, **17**, 181 (2008).
17J. Akedo. *JTTEE5*, **17**, 181 (2007).
18J. Akedo, *J. Am. Ceram. Soc*., **89**, 1834 (2006).
19Y. Imanaka, N. Hayashi, M. Takenouchi, and J. Akedo, *Proc. of Ceramic Interconnect and Ceramic Microsystems Technologies*, 2006.
20Y. Imanaka, N. Hayashi, M. Takenouchi, and J. Akedo, *J. Euro. Ceram. Soc*. **27**, 2789 (2007).
21Y. Kawakami, H. Yoshikawa, K. Komagata, and J. Akedo, *J. Crys. Growth*. **275**, el295 (2005).
22J. Akedo and M. Lebedev, "Piezoelectric Properties and Poling Effect of Pb(Zr, Ti)O_3 Thick Films Prepared for Microactuators by Aerosol Deposition," *Appl. Phys. Lett*. 77, 2000, p. 1710.
23S. Sugimoto, T. Maeda, R. Kobayashi, J. Akedo, M. Lebedev, and K. Inomata, *IEEE Trans. Magnetics.* **39**, 2986 (2003).
24S. Sugimoto, T. Maki, T. Kagotani, J. Akedo, and K. Inomata, *J. Magn. Magn. Mater*. **290-291**, 1202 (2005).
25H. park, J. Kwon, I. Lee, and C. Lee, *Scripta Materialia*, **100**, 44 (2015).
26M. Schubert, J. Exner, and R. Moos, *Materials,* **7**, 5633 (2014).
27D.W. Lee and S.M. Nam, *J. Ceram. Process. Res*. **11**, 100 (2010).
28S.H. Cho and Y.J. Yoon, *Thin Solid Films*, **547**, 91 (2013).
29Y.J. Heo H.T. Kim, K.J. Kim, S. Nahm, Y.J. Yoon, and J. Kim, *Appl. Therm. Eng*. **50**, 799 (2013).
30J. Exner, P. Fuierer, and R. Moos, *J. Am. Ceram. Soc*. **98**, 717 (2015).
31W.E. Lee and K.P.D. Lagerlof, *J. Electron Microscopy Technique*. **2**, 247 (1985).
32J.D. Snow and A.H. Heuer , *J. Am. Ceram. Soc.*, **56**, 153 (1973).
33M.L. Kronberg , *Acta Metall*., **5**, 508 (1957).
34A.H. Heuer , *Phil. Mag*., **13**, 379 (1966).
35*Deformation of Ceramic Materials* edited by R.C. Bradt and R.E. Tressler (Plenum Press, New York, 1975)
36N.I. Tymiak and W.W. Gerberich, *Phil. Mag*., **87**, 5143 (2007).
37N.I. Tymiak and W.W. Gerberich, *Phil. Mag*., **87**, 5169 (2007).
38R. Nowak, T. Sekino, and K. Niihara, *Phil. Mag. A*, **74**, 171 (1996).
39J.D. Clayton, *Proc. Of the Royal Soc. A.,* **465**, 307 (2009).
40E.R. Dobrovinskaya, L.A. Lytvynov, and V. Pishchik, *Sapphire* (Springer, Boston, MA 2009).
41K.P.D. Lagerlof, A.H. Heuer, J. Castaing, J.P. Riviere, and T.E. Mitchell, *J. Am. Ceram. Soc.*, **77**, 385 (1994).
42A. Nakamura, T. Yamamoto, and Y. Ikuhara, *Acta Mater*., **50**, 101 (2002).
43T. Geipel, K.P.D. Lagerlof, P. Pirouz, and A.H. Heuer, *Acta Matall. et Mater*., **42**, 1367 (1994).
44K. Hattar, D.C. Bufford, and D.L. Buller, *Nuclear Instruments and Methods in Physics Research B*. **338**, 56 (2014).
45K. Zhen, C. Wang, Y.-Q. Cheng, Y. Yue, X. Han, Z. Zhang, Z. Shan, S.X. Mao, M. Ye, Y. Yin, and E. Ma. Nature Communications | 1:24 | DOI: 10.1038/ncomms1021
46W.M. Mook, J.D. Nowak, C.R. Perry, C.B. Carter, R. Mukherjee, S.L. Girshick, P.H. McMurry, and W.W. Gerberich, *Phys Rev B*, 75, 2007, pp. 214112-1-10.
47*Materials Science and Engineering Serving Society* edited by R.P.H. Chang, R. Roy, M. Doyama, and S. Somiya. (Elsevier Science, The Netherlands, 1998).
48D.D. Stauffer, A. Beaber, A. Wagner, O. Ugurlu, J. Nowak, K. Andre Mkhoyan, S. Girshick, and W.W. Gerberich, Acta Mater., **60**, 2471 (2012).

Thank you,
for your attention.

Pylin Sarobol –
psarobo@sandia.gov


Questions
?
6505
Sandia National Laboratories

Sandia National Laboratories

BACK UP SLIDES

Ceramic Particle RT Deformation - Sapphire

- Deformation behavior influenced by *number of internal defects*, temperature, crystal orientation/size. Numbers of pre-existing (immobile) defect scale with size.
- In situ SEM/TEM micro-compression and Molecular Dynamics Simulations

Proposed

	Micron	Sub-micron
# Pre-existing Defects	High	Moderate
Energy Density Input	Low	Moderate
Governing Mechanism(s)	Fracture	Plasticity + Fracture
Response to Compression	Crack initiation & Propagation	Dislocation nucleation, slip, crack initiation & propagation
Compression Testing	SEM	SEM and TEM

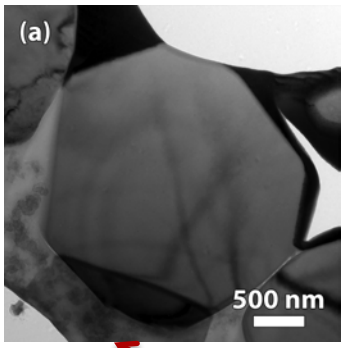

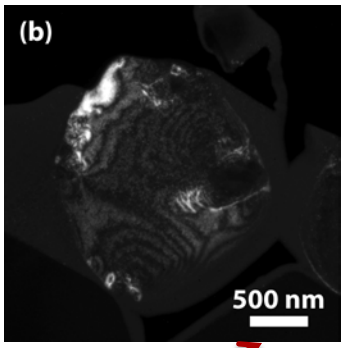

3.0μm Highly Defective

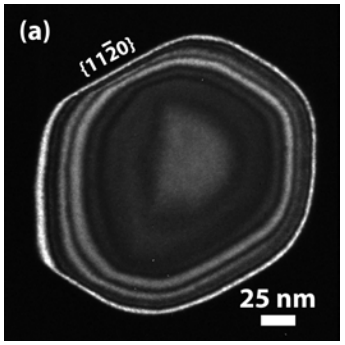

0.3μm Nearly Defect Free

- Infeasible (long computing time) to perform molecular dynamics simulations on size >0.05μm
- 'smaller' particles (0.3μm) are nearly defect-free, and 'larger' particles (3.0μm) contain immobile defects that serve as crack nucleation sites.
- Circumvented the size limitation of our models by simulating similar sized (10 nm) nanoparticles (NPs) that were either
  - single crystal
  - contained a grain boundary (GB) as an initial immobile defect.
- This approach still enables the study of NP deformation/fracture in computationally-feasible systems.

Ceramic Particle RT Deformation - Alumina

Sandia National Laboratories

- Deformation behavior influenced by *number of internal defects*, temperature, crystal orientation/size. Numbers of pre-existing (immobile) defect scale with size.
- In situ SEM/TEM micro-compression and Molecular Dynamics Simulations

Proposed

	Micron	Sub-micron	Single Crystal Nano	Bicrystal Nano
# Pre-existing Defects	High	Moderate	None	Grain Boundary
Energy Density Input	Low	Moderate	High	Low
Governing Mechanism(s)	Fracture	Plasticity + Fracture	Plasticity	Fracture
Response to Compression	Crack initiation & Propagation	Dislocation nucleation, slip, crack initiation & propagation	Dislocation nucleation, Slip	Crack initiation & propagation
Compression Testing	SEM	SEM and TEM	MD Simulation	MD Simulation

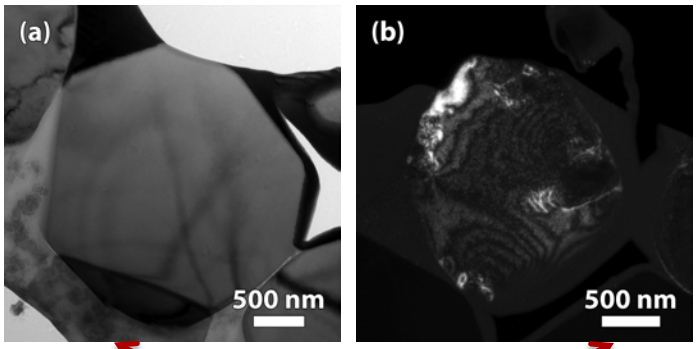

3.0μm Highly Defective

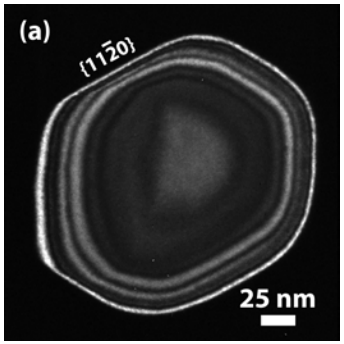

0.3μm Nearly Defect Free

Spherical Particles

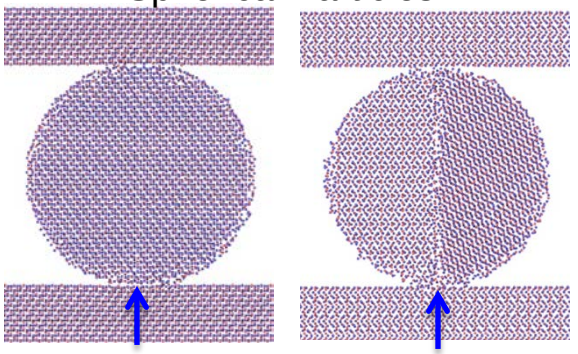

10 nm Defect Free

10 nm with a GB

In Situ SEM micro-compression – 3.0 µm

Sandia National Laboratories

Displacement control, Strain rate ~ 0.003 s^{-1}

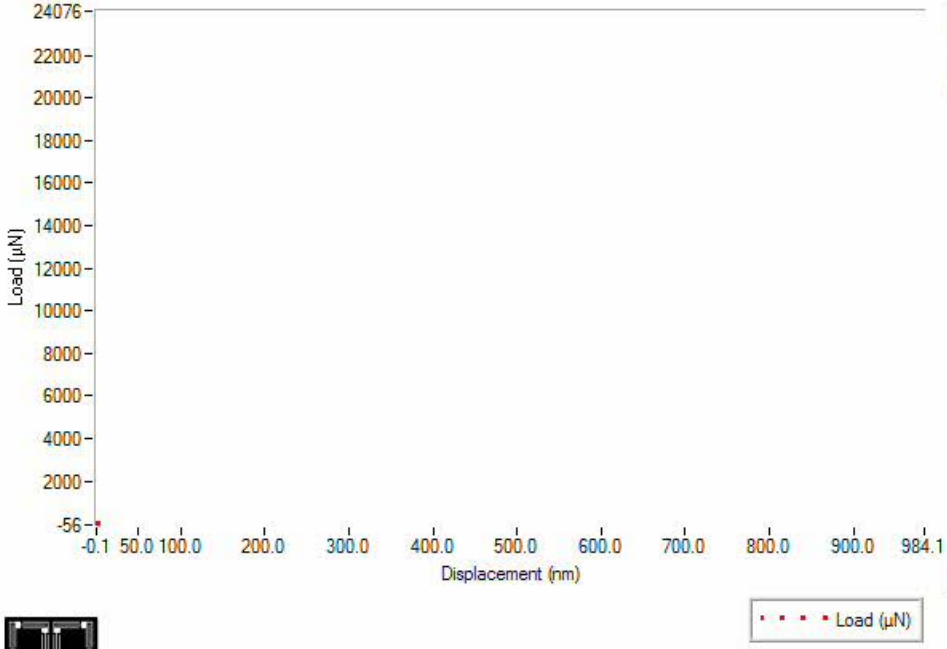

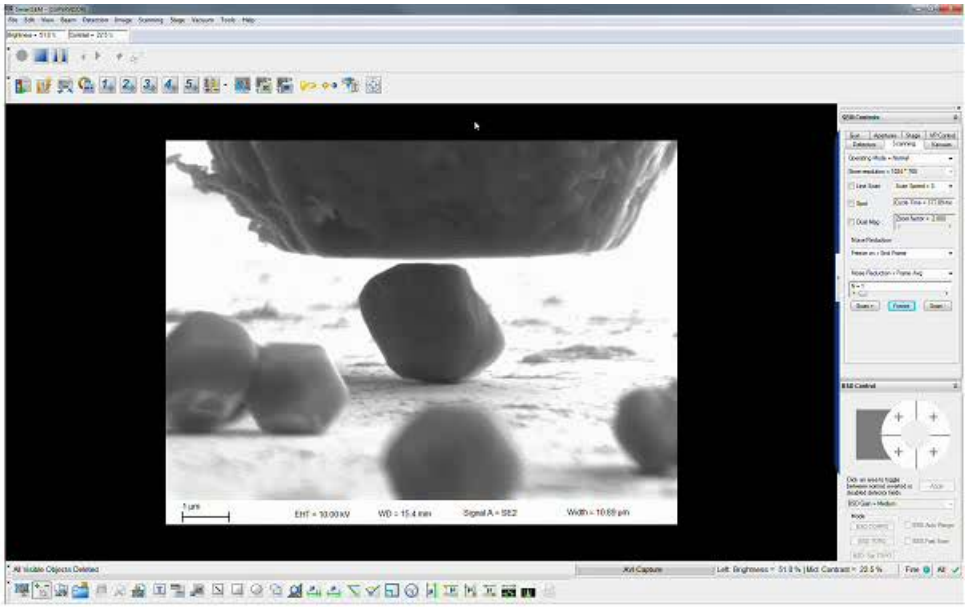

HYSITRON™

- Compressed 4 particles
- No observable shape change prior to fracture and fragmentation
- Displacement excursion corresponded to a fast fracture event
- Strain Energy Density before Fracture ~203 MJ/m^3
- Strain at fracture ~7%

Tip could not keep up with large displacement gained during fracture.

In Situ SEM micro-compression – 0.3 µm

Sandia National Laboratories

Displacement control, Strain rate ~ 0.05 s^{-1}

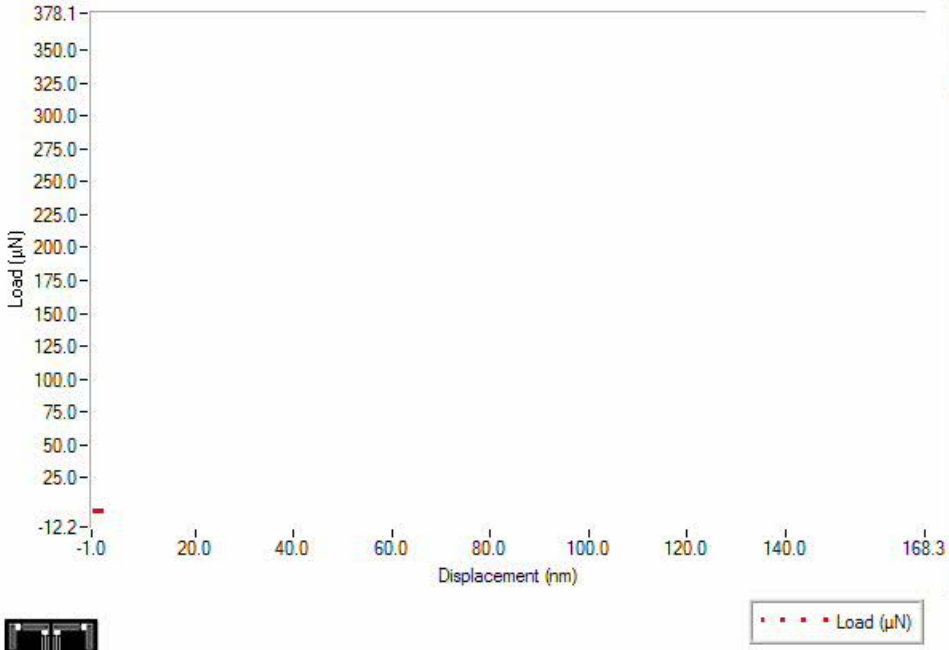

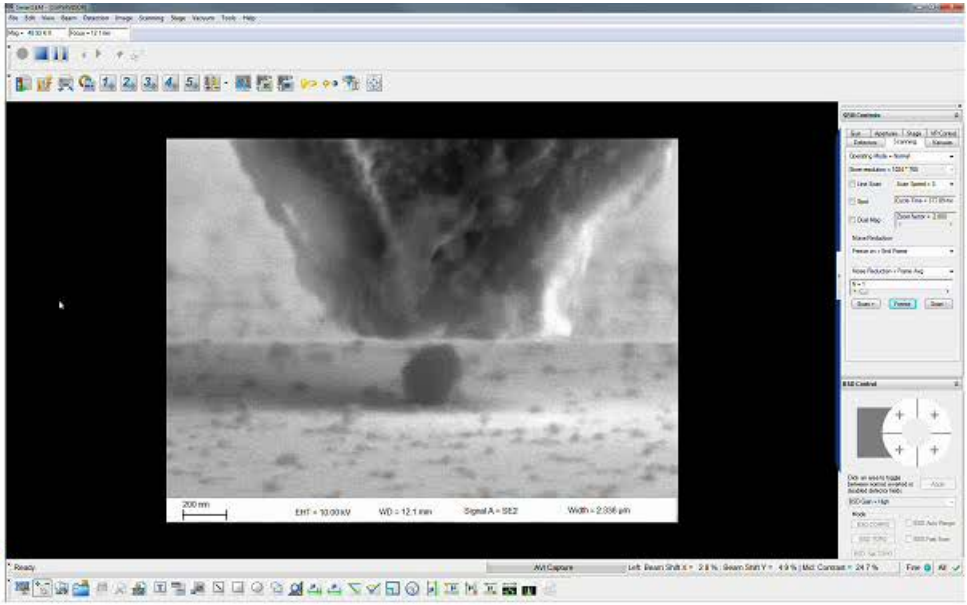

HYSITRON™

- Compressed 4 particles
- Significant plastic deformation/ shape change and stayed intact
- Displacement excursion corresponded to??? *Ex situ* observation
- Strain Energy Density before displacement excursion ~675 MJ/m^3
- Strain at displacement excursion ~16%

Tip could not keep up with large displacement gained during fracture.

Ex Situ SEM observation – 0.3 µm

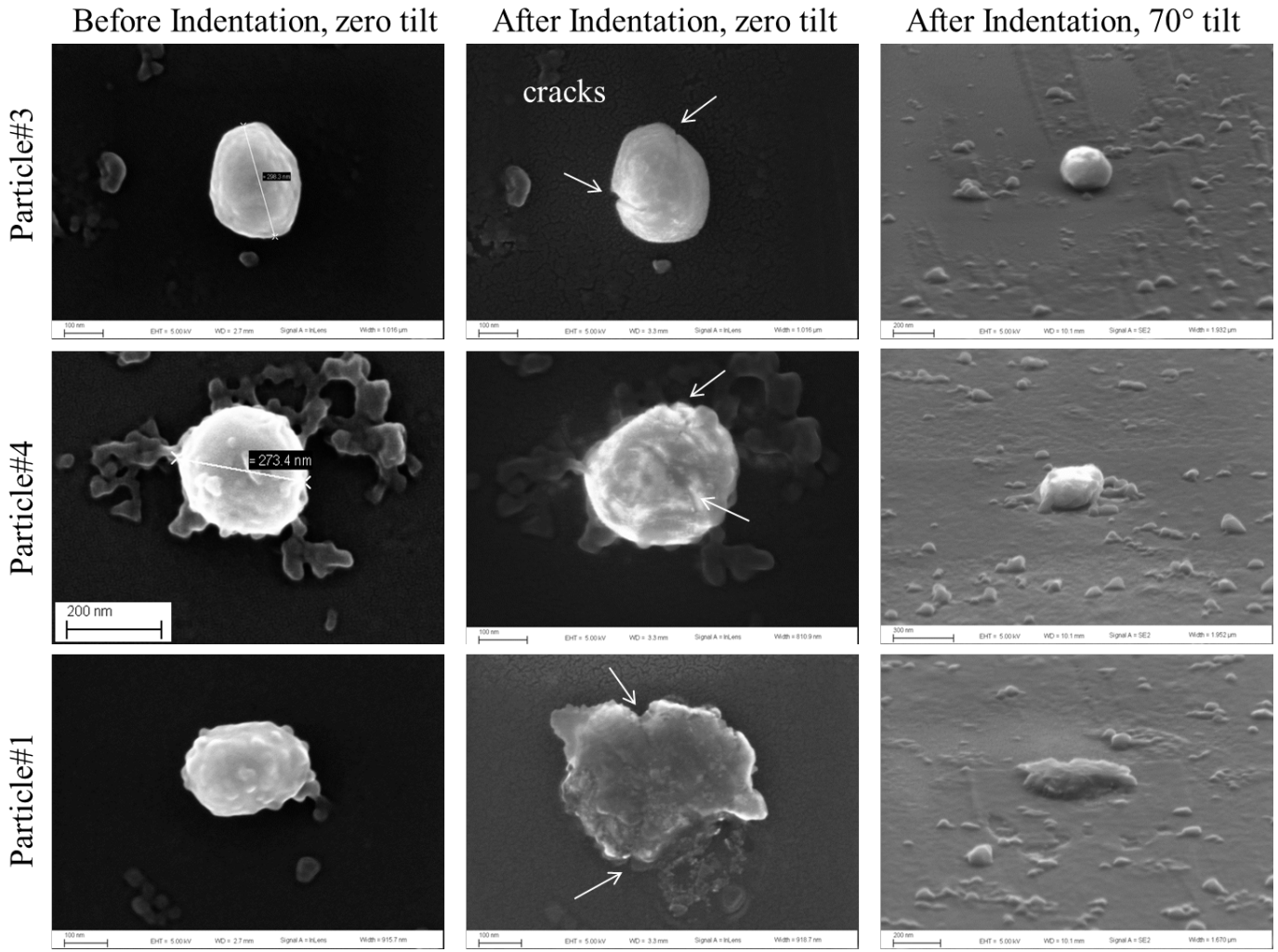

~307 µN
Max load

~420 µN
Max load

Extreme
Loading

Different deformation behavior and load at first fracture may differ from particle-to-particle due to orientation differences and different pre-existing defect densities. However, overall, the sub-micron sized alumina particles exhibited significant plastic deformation before fracture.

Micro-compression Summary

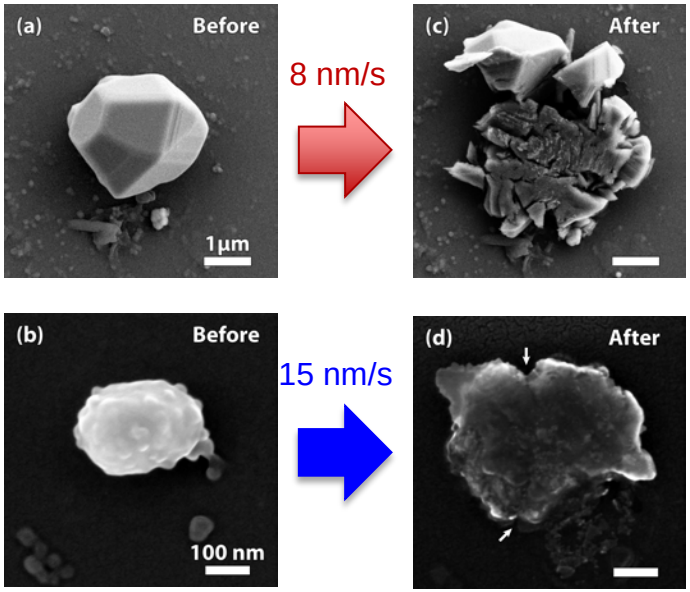

Particle Identifier	Diameter (μm)	Nominal Strain Rate (s^{-1})	Strain Energy Density Before Displacement Excursion (MJ/m^3)	Strain at displacement excursion (%)
Large Particles				
SEM-LP1	2.9	0.03	47	5
SEM-LP2	2.6	0.006	106	5
SEM-LP4	2.9	0.005	70	5
SEM-LP5	2.9	0.003	203	7
Avg Large Particles	**2.8**	-	**106±69**	**5.5 ± 1**
Small Particles				
SEM-SP2	0.17	0.09	494	11
SEM-SP3	0.29	0.05	366	12
SEM-SP4	0.28	0.05	607	13
SEM-SP5	0.29	0.05	675	16
*TEM-SA2	0.38	*0.005	573	32
*TEM-SB1	0.24	*0.009	1066	27
Avg Small Particles	**0.26**	-	**630±238**	**18 ± 9**

	Micron	Sub-micron
# Pre-existing Defects	High	Moderate
Energy Density Input	Low	Moderate
Governing Mechanism(s)	Fracture	Plasticity + Fracture
Response to Compression	Crack initiation & Propagation	Dislocation nucleation, slip, crack initiation & propagation

- Micron sized particles - brittle fracture
- Sub-micron sized particles - substantial plastic deformation before fracture and/or coordinated shear deformation.
  - **6x** higher strain energy density input
    - dislocation nucleation
  - **3x** higher accumulated strain
  - In some cases, became polycrystalline.

Ceramic Particle RT Deformation - Alumina

- Deformation behavior influenced by numbers of internal defects, orientation, size.

Verified

	Micron	Sub-micron	Single Crystal Nano	Bicrystal Nano
# Pre-existing Defects	High	Moderate	None	Grain Boundary
Energy Density Input	Low	Moderate	High	Low
Governing Mechanism(s)	Fracture	Plasticity + Fracture	Plasticity	Fracture
Response to Compression	Crack initiation & Propagation	Dislocation nucleation, slip, crack initiation & propagation	Dislocation nucleation, Slip	Crack initiation & propagation
Compression Testing	SEM	SEM and TEM	MD Simulation	MD Simulation

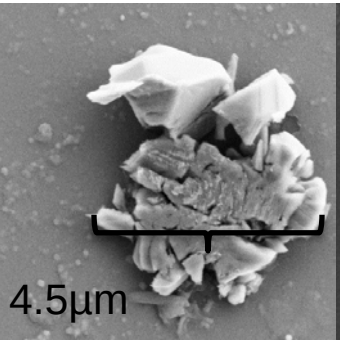

3.0µm - Fracture and Fragmentation

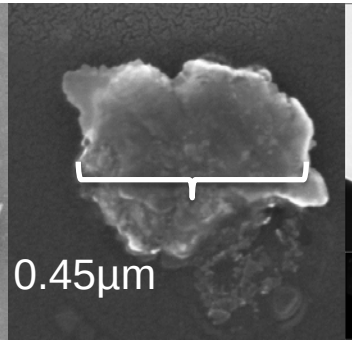

0.3µm – plastic deformation, shape change, cracking

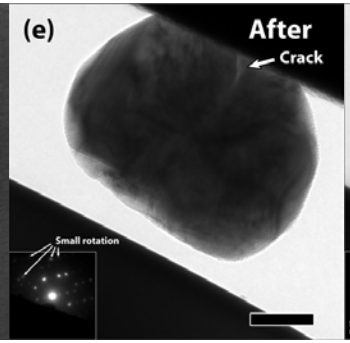

0.3µm - Dislocation Plasticity & through particle fracture

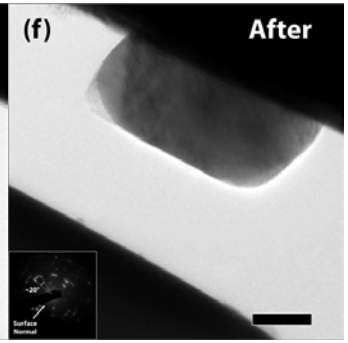

0.3µm - Coordinated Shear Deformation - Polycrystalline

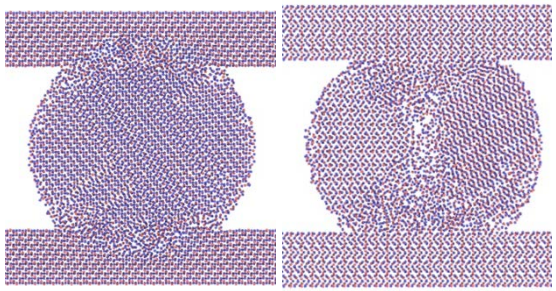

10 nm - Coordinated Shear Deformation **10 nm - Fracture**